Hale, Layton C. "Principles and techniques for desiging precision machines." PhD Thesis, 1999.

2.6 Exact-Constraint Design

By “dusting off” the principles of kinematics and applying them to machine design, we arrive at the method of *Exact Constraint*. The method of Exact Constraint has been developed to the point where it comprises a body of knowledge which can be used to routinely create new machine designs which are both high in performance and low in cost. The results are so excellent, yet so obvious; so elegant, yet so simple; that at once they seem

> both profound and trivial! Perhaps it is this duality which has kept these principles so well hidden. One may ask: "Of what value could anything so trivial be?" And so these principles have been overlooked. They have become disused.
>
> [Blanding, 1992]

The designers of mechanisms routinely use the principles of kinematics because overconstrained or underconstrained devices simply will not function. What the precision engineer must remember is that at some scale, everything is a mechanism. The component that must remain stable to nanometers will not if it is overconstrained to a structure that deforms by micrometers. This is often the most important motivation for exact-constraint or kinematic design in precision machines, that is, to isolate sensitive parts or systems such as a metrology frame from the influence of dimensionally changing supports and/or manufacturing tolerances.[I] Similarly, parts will fit together precisely and without backlash if they are exactly constrained, for example, kinematic couplings. This is why [Smith and Chetwynd, 1992] state that "a divergence from pure kinematic design results in increased manufacturing costs."[II]

The term exact constraint is very explicit and meaningful once the basic concept is understood. An unconstrained *rigid* object has six degrees of freedom usually identified as three translations and three rotations. A *nonrigid* object may have one or more degrees of flexibility that act as additional degrees of freedom, relatively speaking. For example, an open shoe box is torsionally flexible and so would have a total of seven degrees of freedom. The proper application of constraints would eliminate degrees of freedom in a one-to-one fashion. It is the objective of exact-constraint design to achieve some desired freedom of motion or perhaps no motion by applying the minimum number of constraints required. Often we conceptualize in terms of an *ideal* constraint, which is absolutely rigid against motion in one or more degrees of freedom and is absolutely free in the remaining degrees of freedom. A *real* constraint such as a small-area contact between surfaces, a link or a bearing, provides one or more degrees of constraint that are relatively much stiffer than the degrees of freedom and so approximates ideal behavior.[III]

The reference by Blanding is an excellent introduction to exact-constraint design and rigid structures. Because it is so basic and complete, it forms the basis for this

---

[I] The word kinematic is more often used, but exact constraint is more descriptive and thus is preferred.

[II] As a practical matter, purely kinematic designs are generally difficult to achieve; whereas, so called semi-kinematic designs (for example, Hertzian contact areas instead of frictionless point contacts) generally provide acceptable isolation characteristics, greater robustness and lower cost. The quotation might better read "a divergence from kinematic design theory may result in increased manufacturing costs." As an alternative, the process of replication produces a good fit and is relatively low in cost.

[III] In the case of a sliding bearing or small-area contact, the degree of freedom may be as stiff as the constraint until sliding occurs. Ideal behavior requires that the frictional force divided by the constraint stiffness be a negligible deflection.

introductory section. Several other references provide accounts of more specific exact-constraint designs such as [Slocum, 1992], [Smith and Chetwynd, 1992], and [Furse, 1981]. In addition, Chapter 6 provides a thorough treatment of exact-constraint design, and examples of exact-constraint designs appear in Chapter 7. In this section, however, the basic concepts are introduced through statements that appear in [Blanding, 1992]. Although these statements deal specifically with *ideal* constraints, they provide the essential understanding of kinematics required for the design of *real* constraint systems. Following each statement is an explanation to reinforce and sometimes extend its meaning. The point here is to understand and visualize basic kinematic techniques rather than to apply a bunch of rules that are easy to forget.

Statement 1: Points on the object along the constraint line can move only at right angles to the constraint line, not along it.

A single-degree constraint prevents motion in one direction, the constraint direction, represented by a line in space. The only component of motion allowed by the constraint is perpendicular to the constraint line. If the object is rigid, then all points of the object along the constraint line are so constrained. The initial or so called instantaneous motion is always perpendicular to the constraint direction (for ideal constraints). The constraint direction may change as the object moves in which case the constrained path is curved and the instantaneous motion is tangent to the curve. For example, any point on a wheel with a fixed axle is constrained to a circular path. The constraint direction is radial and the instantaneous motion is tangent to the circle.

Statement 2: Any constraint along a given constraint line is functionally equivalent to any other constraint along the same constraint line (for small motions).

By Statement 1, the instantaneous motion is always perpendicular to the constraint line irrespective of the actual constraint. It follows that any constraint on a given constraint line produces the same instantaneous motion. For small motions about an operating point, the curved path of motion produced by any constraint on the given line is approximately equal to the instantaneous motion (or tangent) at the operating point. Thus, any two constraints on the same constraint line are approximately equal for small motions.

Statement 3: Any pair of constraints whose constraint lines intersect at a given point, is functionally equivalent to any other pair in the same plane whose constraint lines intersect at the same point. This is true for small motions and where the two constraints lie on distinctly different constraint lines.[I]

[I] The final sentence in Statement 3 was changed from “This is true for small motions and where the angle between constraints does not approach 0° (180°)” to allow the possibility of parallel constraints that effectively intersect at infinity.

The intersection described by this statement is an instantaneous center of rotation, or simply an instant center. The reduction of a constraint pair (or triple) to an instant center is an important visual and conceptual aid in the field of kinematics. We must distinguish, however, between the stationary point that is on or relative to the constrained body and the instant center that lies momentarily at this point. The point on the body can have only instantaneous motion that is perpendicular to the plane formed by the two constraints. In this plane the point will appear stationary for small motions while the instant center will appear to move with the moving constraint directions. Any pair of constraints that lie in this plane and intersect the same point will allow the same instantaneous motion of that point on the body; however, the motion of the instant center may be quite different. Any other point on the body may have an additional, tangential component of instantaneous motion about the instant center, as shown in Figure 2-16 (a).

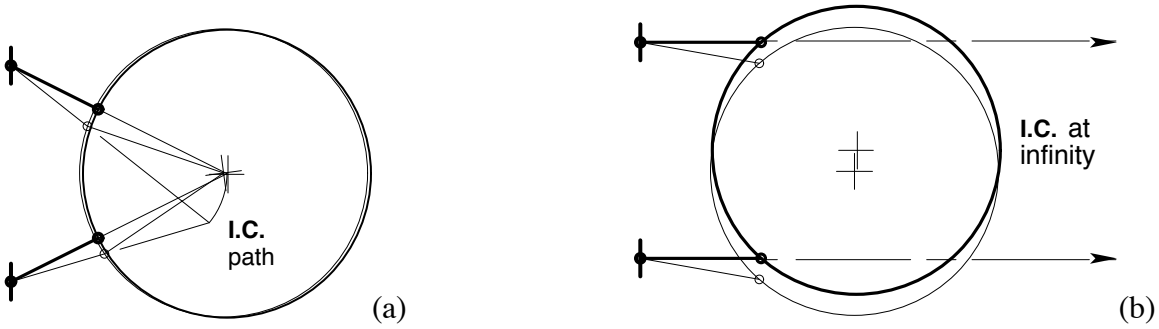

Figure 2-16 In (a), the instant center is momentarily located at the physical center of the circle (heavy lines). The instant center moves down (light lines) while the circle rotates approximately about its physical center. In (b), the instant center is off at infinity and the circle initially translates downward.

The condition that the two constraint lines be distinctly different requires further explanation as it leads to a key concept. If two constraints were to lie on a single line, then they would not define a plane and the statement would not make sense. The physical result would be one overconstrained degree of freedom rather than two constrained degrees of freedom. An acceptable case, however, is two parallel constraints that are separate and thus define a plane. As Figure 2-16 (b) indicates, we may consider parallel constraint lines to intersect at infinity such as railroad tracks appear at a distance. An object that rotates about a distant center appears to translate such as a ship appears as it rotates about the center of the Earth. With this background, we may conceptualize three translations and three rotations as being equivalent to six rotational degrees of freedom where three axes are at infinity.

Statement 4: The axes of a body's rotational degrees of freedom will each intersect all constraints applied to the body.[I]

[I] This is true if each axis provides uncoupled rotation. An example of coupling is the rotation of a lead screw with its associated translation. The consequence of violating Statement 4 is more complex motion.

This is a very powerful and comprehensive statement that uses explicitly the representation of translations as rotational axes located at infinity. It is a generalization of the instant center and is valuable as a visual aid to understanding a mechanism or in synthesizing the system of constraints for a new mechanism. The proof of this statement is quite trivial. If there exists an axis that intersects all applied constraint lines, then no constraint exists that can affect a moment about that axis because the lever arm is zero. Hence, the body is free to rotate about that axis, as demonstrated in Figure 2-17.

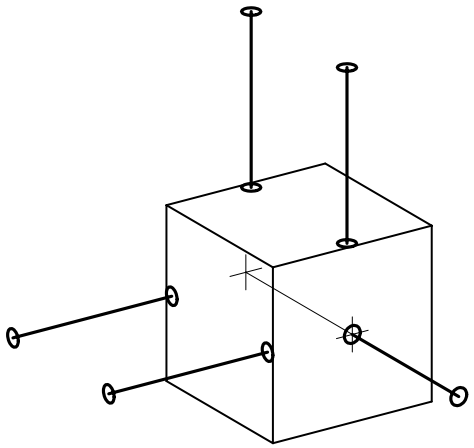

Figure 2-17 All five applied constraints intersect the only remaining degree of freedom, a rotation about the center of the cube.

Statement 5: A constraint applied to a body removes that rotational degree of freedom about which it exerts a moment.

In order to constrain a rotational degree of freedom (which includes translations by equivalency), the constraint must react with a moment about the axis of rotation. A constraint will satisfy this requirement if the constraint line does not intersect the axis of rotation and if the constraint line is not parallel to the axis of rotation.[I] An exception to the first condition will result in a zero-length lever arm. An exception to the second condition will result in a moment that has no component along the axis of rotation. Figure 2-18 shows the addition of a third constraint to prevent rotation of the circle about its center. Each constraint prevents rotation about the instant center formed by the other pair of constraints so that three degrees of freedom are exactly constrained. The axes of the remaining three rotational degrees of freedom will each intersect all three constraints per Statement 4. If the three constraints happen to lie in the plane of the figure, then so too will the axes of rotational freedoms.

[I] Just as parallel constraints intersect at infinity, an axis of rotation and a constraint line that are parallel to each other also intersect at infinity.

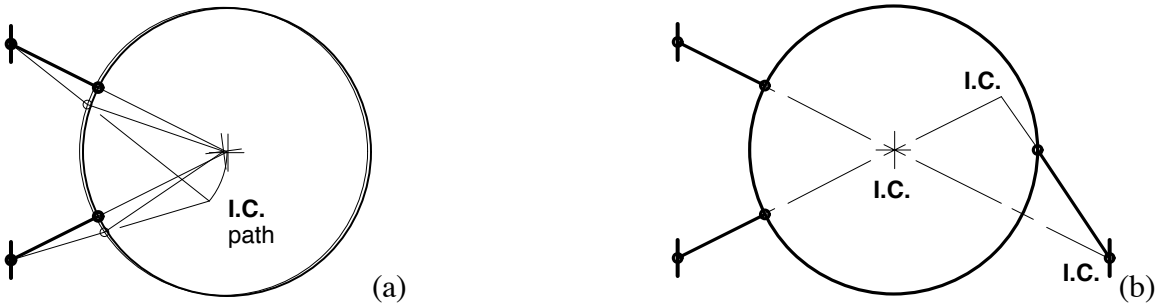

Figure 2-18 The rotational freedom of the circle about its center in (a) is constrained in (b) by the addition of a constraint that reacts with a moment about the center. Each constraint reacts with a moment about an instant center formed by the other pair of constraints.

The length of the lever arm, that is, a perpendicular drawn from the constraint line to the constrained rotational axis, is a relative measure of the effectiveness of that constraint. If one is seeking a balanced design, then a sensible approach is to seek lever arms having nearly equal length. This leads to a simple rule of thumb for planar problems; *arrange constraint lines to form an equilateral triangle*, as shown in Figure 2-19. Of course there may be valid reasons to choose different angles. Many three dimensional problems have a planar nature, which greatly helps visualization.

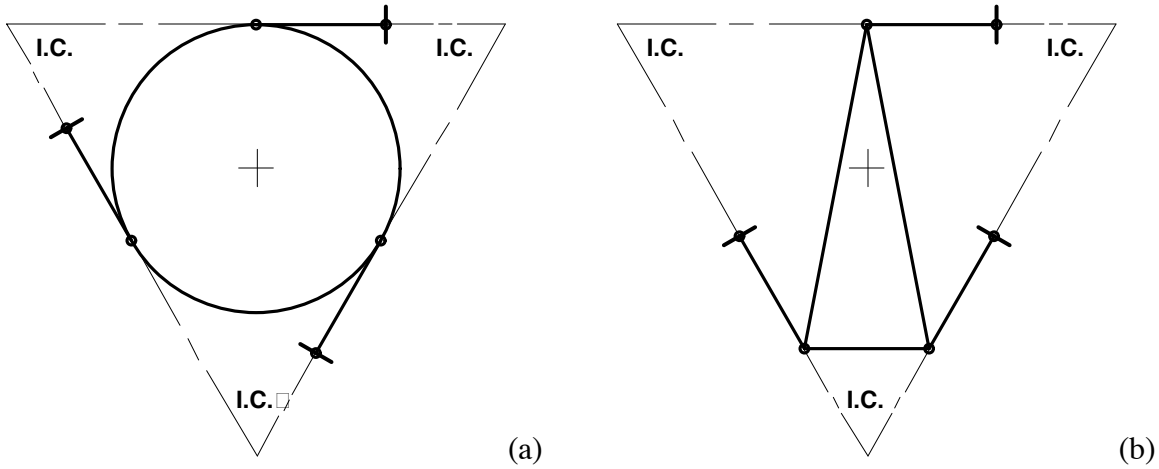

Figure 2-19 An equilateral arrangement of constraints often provides a better balance of stiffness. In (a) the center of stiffness lies at the center of the circle, and the vertical and horizontal stiffnesses are equal. The center of the triangular object in (b) is somewhat lower than the center of stiffness. A slightly wider angular spacing between the lower two constraints would lower the center of stiffness while increasing the horizontal stiffness and decreasing the vertical stiffness.

Statement 6: Any set of constraints whose constraint lines intersect a complete and independent set of rotational axes, is functionally equivalent to any other set of constraints whose constraint lines intersect the same or equivalent set of

rotational axes. This is true for small motions and when each set contains the same number of independent constraints.[I]

This is an extension of Statement 3, *the functional equivalence of any constraint pair having the same instant center*, based on Statement 4, *the generalization of the instant center to a rotational axis*. The statement is most meaningful and useful when the constraints total four or more, as at least two pairs of constraints are required to uniquely define an axis of rotation. The examples shown in Figure 2-20 are functionally equivalent (for small motions) to each other and to the example in Figure 2-17. Each has five constraints that uniquely define the same axis of rotation. It is natural to ask if there are any other arrangements of five constraints that will define the same axis of rotation. Blanding has developed a chart of all possible orthogonal constraints involving one to six constraints. Re-created in Figure 2-21, the orthogonal constraint chart provides an excellent starting point for any exact-constraint design.[II] An infinite number of nonorthogonal configurations is possible based on these basic configurations. Categories where a constraint arrangement does not exist usually require a series combination of constraint systems.

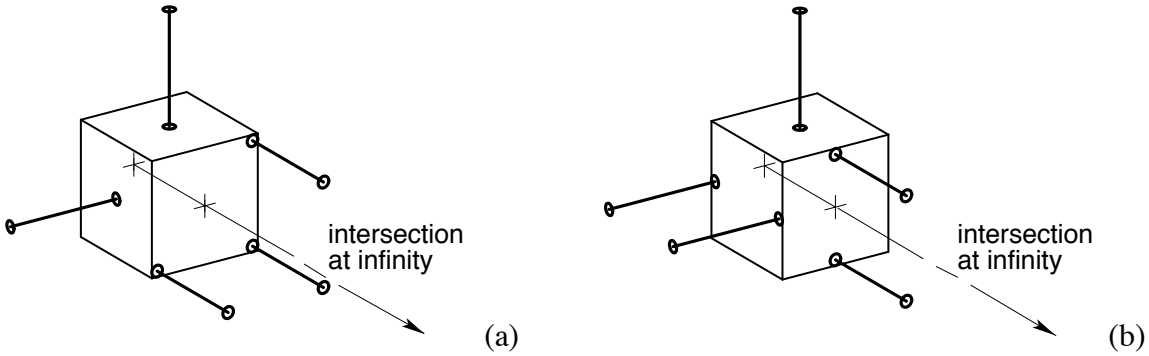

Figure 2-20 In both (a) and (b), all the applied constraints intersect the only remaining degree of freedom, a rotation about the center of the cube. These two constraint cases are functionally equivalent since all the constraints intersect the same rotational axis.

[I] Statement 6 was changed from "Each of a body's remaining rotational degrees of freedom is intersected by the line(s) of any applied constraint(s)" because it provided no new information beyond Statement 4. The definition of "equivalent sets of rotational axes" comes later in Statements 10 and 11.

[II] Blanding's original chart numbers the cells according to constraints rather than degrees of freedom and does not show the centerlines and arrows to help in visualizing the degrees of freedom.

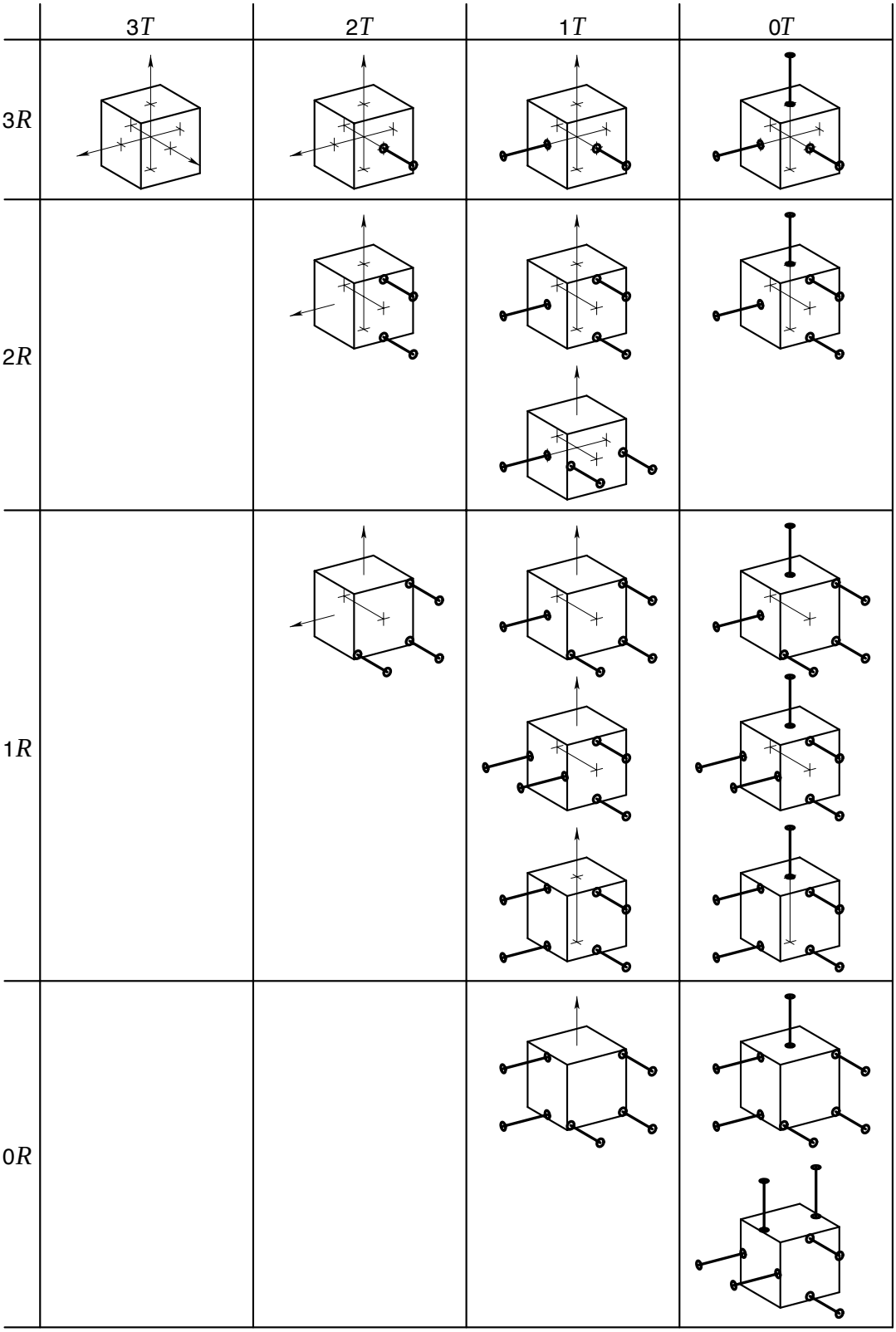

Figure 2-21 A matrix of desired rotational degrees of freedom (centerlines) and translational degrees of freedom (arrows) shows all possible orthogonal constraint arrangements, after [Blanding, 1992].

Statement 7: An *Ideal Sheet Flexure* imposes absolutely rigid constraint in its own plane (X, Y, and θ_Z), but it allows three degrees of freedom: Z, θ_X, and θ_Y.

A sheet flexure, more commonly called a blade flexure, is one of the most important constraint devices used in precision machines. A blade flexure allows out-of-plane motion while resisting in-plane motion as Figure 2-22 clearly shows. The equivalent three-constraint system superimposed on the flexure serves only as a conceptual aid. We know from experience that a thin blade is very compliant for out-of-plane bending. Equations 2.19 through 2.22 give the stiffnesses for the directions that are usually most relevant.[I] For a given axial stiffness, the moment stiffness varies as the square of the blade thickness. The desire to minimize blade thickness will invariably require much greater width than thickness so there is sufficient cross sectional area to carry the load and/or to provide axial stiffness. Generally, the size constraint on a blade flexure will be either the maximum width or the minimum thickness. Blade length affects moment stiffness and axial stiffness the same way and so is driven by other considerations. Usually the length to thickness ratio is limited to 10:1 for typical materials to avoid buckling. Equation 2.23 gives the condition required for the blade to yield before buckling. A blade sized to resist buckling usually is too short to have adequate translational freedom. In this case, two short blades spaced apart in the same plane and connected by a larger bar section will provide greater translational compliance by the square of the separation distance.[II] To the extent that the blade bends as a hinge, the bending stress is approximately constant over the length and given by Equation 2.24. Combining the stress and buckling relations leads to a bound on bending angle due only to material properties as expressed in Equation 2.25. An angle of 3° is reasonable for hardened steel but the resistance to buckling decreases with angle. The material parameters E, ν and σ_y represent elastic modulus, Poisson ratio and yield strength, respectively.

$$k_x = \frac{E \cdot t \cdot w}{a} \tag{2.19}$$

$$k_z = \frac{k_x\, t^2}{\left(1-\nu^2\right)a^2 + 2.4(1+\nu)t^2} \tag{2.20}$$

$$k_{\theta_y} = \frac{k_x\, t^2}{12\left(1-\nu^2\right)} \tag{2.21}$$

[I] Finite element studies of typical blade flexures reveal that plane stress better approximates axial stiffness while plane strain better approximates bending stiffness. As a result, these formulas lead to slighly more conservative designs. See Chapter 6.2 for further details and derivations.

[II] See Statements 11 and 12 for further explanation.

$$k_{\theta_x} = \frac{k_x t^2}{12}\left[\frac{1}{2(1+\nu)\left(4 + 2.52\frac{t}{w}\right) + \frac{w^2}{\left(1-\nu^2\right)a^2 + 2.4(1+\nu)t^2}}\right] \tag{2.22}$$

$$\frac{a}{t} < \pi\sqrt{\frac{E}{12\sigma_y}} \tag{2.23}$$

$$\sigma_b = \frac{E \cdot t}{2a}\theta = \frac{k_x}{2w}\theta \tag{2.24}$$

$$\theta < \pi\sqrt{\frac{\sigma_y}{3E}} \tag{2.25}$$

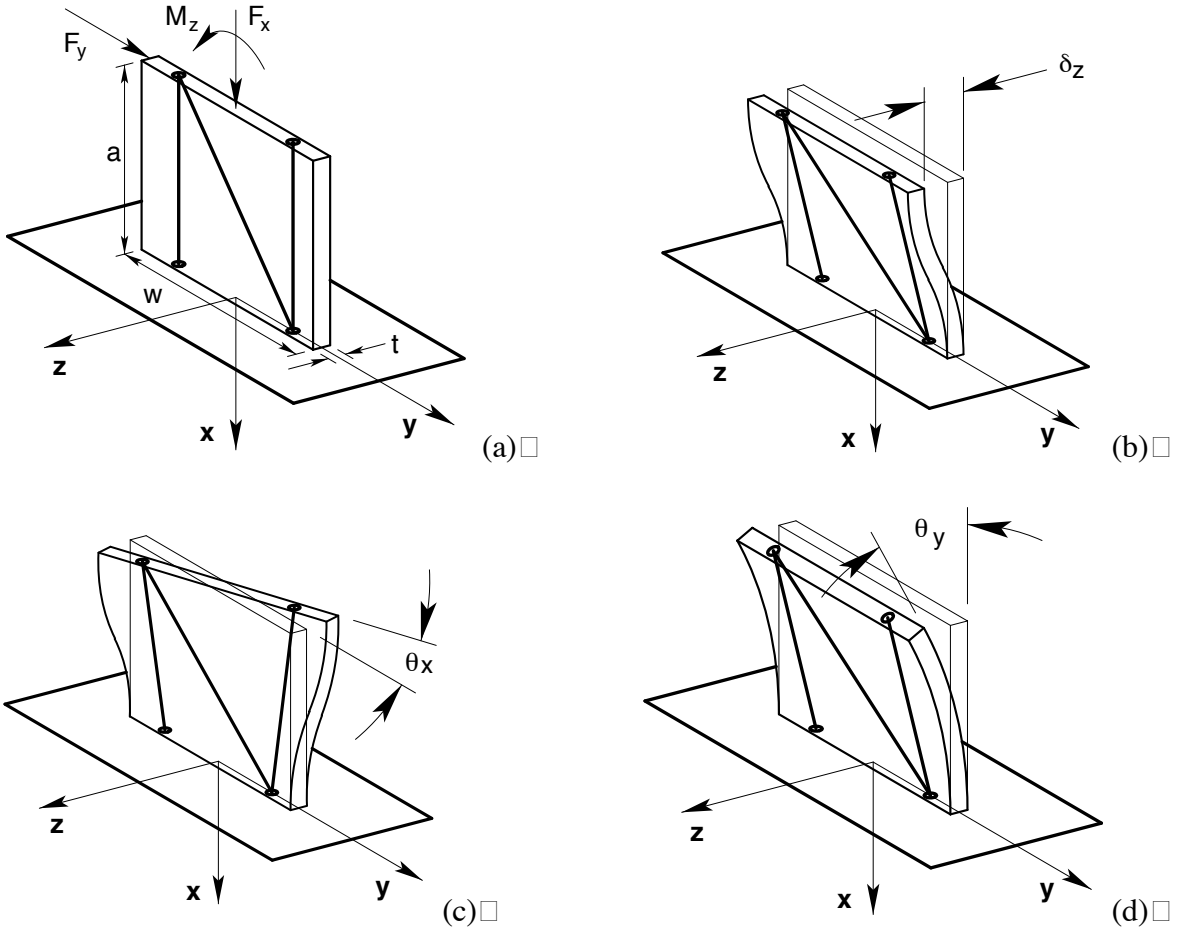

Figure 2-22 A blade flexure provides constraint against forces and moments in the plane of the blade (a). A blade flexure provides freedom to small motions in bending modes of the blade (b, c, d). The blade is represented equivalently by three single-degree constraints as shown.

Statement 8: An *Ideal Wire Flexure* imposes absolutely rigid constraint along its axis (X), but it allows five degrees of freedom: Y, Z, θ_x, θ_y, θ_z.

This is the ideal constraint that has become so familiar by now. Often two wires are used in opposition to constrain a single degree of freedom. Such a configuration resists buckling and doubles the axial stiffness if the wires have pretension. Pretension has the adverse effect of increasing lateral stiffness by the ratio of tension to length for each wire. A better alternative is simply to limit the length to diameter ratio to approximately 10:1, thereby stiffening translation to better resist buckling. To recover translational freedoms, two short wires spaced along the constraint line and connected by a larger section rod will provide greater translational compliance by the square of the separation distance.

> Statement 9: A constraint ($\mathcal{C}$) properly applied to a body (i.e., without overconstraint) has the effect of removing one of the body's rotational degrees of freedom ($\mathcal{R}$'s). The $\mathcal{R}$ removed is the one about which the constraint exerts a moment. A body constrained by n constraints will have $6-n$ rotational degrees of freedom, each positioned such that no constraint exerts a moment about it. In other words, each $\mathcal{R}$ will intersect all $\mathcal{C}$'s.[I]

This is an extension of Statements 4 and 5 that provides a way to test for overconstraint and underconstraint. The first test is simply to count the number of constraints. We can generalize to nonrigid bodes by increasing the number of free-body degrees of freedom by f flexural degrees of freedom. The number of independent $\mathcal{C}$'s required to exactly constrain a body is $n=6+f-d$, where d is the number of desired degrees of freedom. The second test is required to determine whether the $\mathcal{C}$'s are independent. The removal of a redundant $\mathcal{C}$ will not affect the number of degrees of freedom that the remaining $\mathcal{C}$'s allow. The system is exactly constrained if the removal of any single constraint increases the number of degrees of freedom by one. Figure 2-23 provides specific examples of this and the orthogonal constraint chart, Figure 2-21, provides further examples by observing changes between adjacent cells.

Statement 9 as written has one small technical problem that may be discovered when performing the test for independent constraints. A single degree of freedom may consist of a coupled rotation and translation such as the motion described by the lead of a screw. This behavior occurs when a constraint does not intersect the axis of rotation (thus they are not parallel either), thereby introducing translation along the same axis. Figure 2-25 shows an example that demonstrates this behavior. Chapter 6 presents a flexure coupling for ball screws that is designed to have the same lead as the screw.

[I] Blanding uses the notation $\mathcal{R}$, $\mathcal{T}$, $\mathcal{C}$ throughout his book to represent rotational freedom, translational freedom and constraint, respectively. It just happens to show up in Statements 9 through 11.

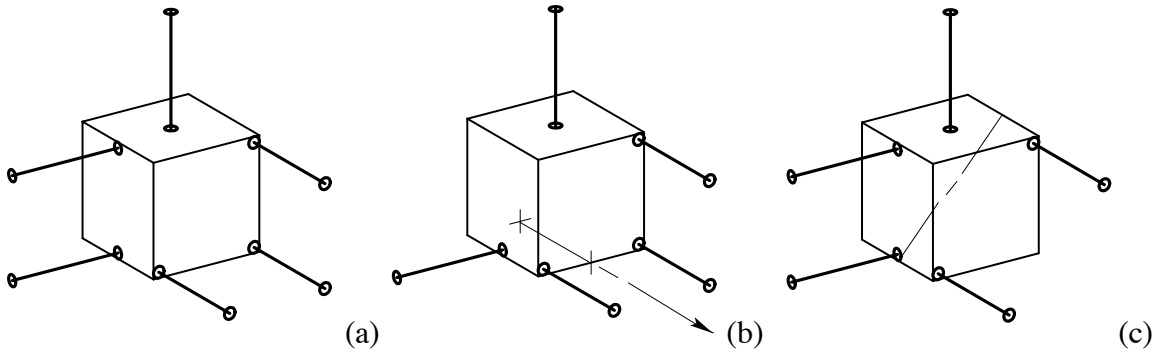

Figure 2-23 To test whether the six constraints in (a) are independent, remove any single constraint and see if a new degree of freedom results. The constraint removed in (b) can no longer exert a moment about the axis shown and neither can the remaining constraints. The same applies to (c) and the remaining cases.

Statement 10: Any pair of intersecting rotational degrees of freedom ($\mathcal{R}$'s) is equivalent to any other pair intersecting at the same point and lying in the same plane. This holds true for small motions.

Another way of stating this is that *a pair of intersecting $\mathcal{R}$'s can generate instantaneous rotation about any axis that lies in the plane and passes through that point*. As Figure 2-24 shows, the constraints that allow this motion must either lie in this plane or intersect the plane where the two $\mathcal{R}$'s intersect by Statement 4. The small motion requirement is necessary even for pure axes of rotation because rotation about one axis changes the orientation of the other. Usually this is not a problem and complicates only the algorithm that computes the angles. A familiar example is Hooke's coupling (the typical universal joint). It transmits shaft power through a bend but its transmission ratio is 2ω cyclic with an amplitude that increases with the square of the angle.

Figure 2-24 The circle lies in the plane of three constraints and the fourth constraint intersects its center. Any distinct pair of rotational axes that lie in this plane and intersect the center will represent the instantaneous motions allowed by the constraints.

Statement 10 extends to the intersection of three $\mathcal{R}$'s so long as each triple spans three-dimensional space. Three $\mathcal{C}$'s that intersect at the same point will allow instantaneous rotation about any axis that passes through that point. Figure 2-25 shows a flexure pivot that has three *nonintersecting* wire constraints. This flexure provides three $\mathcal{R}$'s that span

three-dimensional space, but the motion is more complicated since the $\mathcal{R}$'s do not intersect. This leads to an interesting coupling between rotations and translations, or equivalently between forces and moments. The easiest one to visualize is the rotation about the axis of symmetry causing a translation along the same axis. The consequence of constraints not intersecting the axis of rotation is the motion described by the lead of a screw.

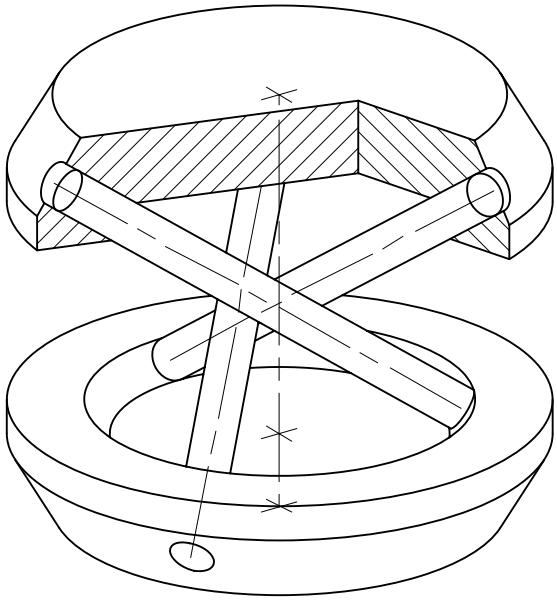

Figure 2-25 This flexure was created by shifting mutually orthogonal wires off center so that they clear one another. The angle of each wire with respect to the center axis is 54.736° (the arc tangent of $\sqrt{2}$). The offset of each wire from center is the desired distance between wire centers divided by $\sqrt{2}$.

Statement 11: Two parallel $\mathcal{R}$'s are equivalent to any two parallel $\mathcal{R}$'s, parallel to the first pair and lying in the same plane. They are also equivalent to a single $\mathcal{R}$ parallel to the first pair and lying in the same plane; and a $\mathcal{T}$ perpendicular to that plane.

This follows from Statement 10 where the point of intersection occurs at infinity. The small motion requirement has been dropped because rotation about one axis does not alter the orientation of a parallel axis, which is a first order effect for nonparallel axes. There is, however, a second order translation that depends inversely upon the distance between the parallel axes. Thus in the strictest sense, there is a small motion requirement.

Statement 12: When parts are connected in series (cascaded), add the degrees of freedom. When the connections occur in parallel, add constraints.[I]

[I] The series addition of functionally equivalent degrees of freedom results in an indeterminacy that may or may not present a problem.

We shall use two familiar rules to explain Statement 12. Rule 1: *The equivalent compliance of springs connected in series is the sum of their individual compliances*. Rule 2: *The equivalent stiffness of springs connected in parallel is the sum of their individual stiffnesses*.[I] We may recall these rules applied to single-degree-of-freedom springs, but they also apply to springs and structures of any dimension, where the spring constant becomes a symmetric matrix. We may consider a degree of freedom as being a dominant term in the compliance matrix whether its origin is the elasticity of a blade flexure or the motion of a bearing. Similarly, we may consider a constraint as being a dominant term in the stiffness matrix. The foundation for Statement 12 is that dominant terms in individual matrices remain dominant through the addition process.[II] Therefore, degrees of freedom dominate through series combinations while constraints dominate through parallel combinations. This exposes a subtlety that is not apparent in Statement 12, namely, how to deal with redundant constraints and degrees of freedom. We will work through these by example starting first with a series combination followed by a parallel combination.

Figure 2-26 (a) shows a series combination of two blades that share a common constraint line. Someone could misinterpret Statement 12 to mean that this series of blades, each with three degrees of freedom, would combine to have a total of six degrees of freedom and no constraints. The combined axial compliance along the constraint line is still orders of magnitude more rigid than the other directions, thus it remains a constraint. Likewise, the blades share a common rotational axis that results in a redundant degree of freedom. The combination may have twice the compliance but functionally remains a single degree of freedom. In the remaining directions, Statement 12 applies without confusion as four degrees of freedom combine with four constraints. In practice, we usually keep the blades short and duplicate another set further down the constraint line to provide much greater translational freedom. It is functionally equivalent to a wire flexure but with much higher axial stiffness and load capacity.

Figure 2-26 (b) shows a more elaborate flexure that has both series and parallel combinations of blades. This design has a hole down the center to prevent a *short circuit* in the desired degrees of freedom. Its symmetry leads to redundant constraints. It could function the same without the redundant constraints (by eliminating the symmetry) but this would sacrifice too much stiffness along its constraint line.

To summarize, the proper way to interpret Statement 12 requires an awareness of the directions involved. For a series combination of parts, the combined degrees of freedom will span the *union* of dimensional spaces spanned by the degrees of freedom of

---

[I] The stiffness of a spring is the load required to produce a unit displacement and the compliance is the inverse of stiffness.

[II] The individual matrices must be of the same size (generally 6 by 6) and with respect to the same coordinate system, which may require multiplication by a coordinate transformation matrix.

the individual parts; whereas, the combined constraints will span the *intersection* of spaces spanned by the constraints of the individual parts. For a parallel combination of parts, the combined constraints will span the *union* of dimensional spaces spanned by the constraints of the individual parts; whereas, the combined degrees of freedom will span the *intersection* of spaces spanned by the degrees of freedom of the individual parts. Fortunately this is easier to understand than it is to phrase.

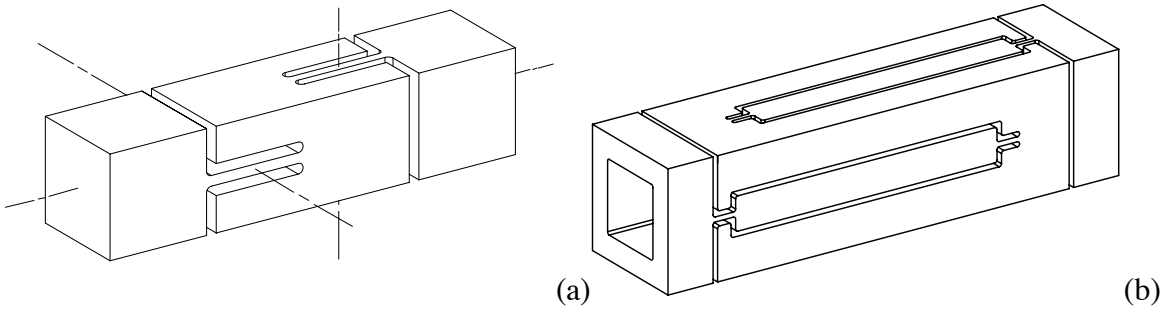

Figure 2-26 In (a), a series combination of two blades provides three independent rotational degrees of freedom and one axial constraint. Cutting these features into each end of a longer bar provides two translational freedoms. In (b), the blades are effectively longer to provide two translational freedoms but a center hole is required to prevent a short circuit around the series of flexures. The cross section could be round rather than square. These monolithic flexures can be manufactured using wire EDM.

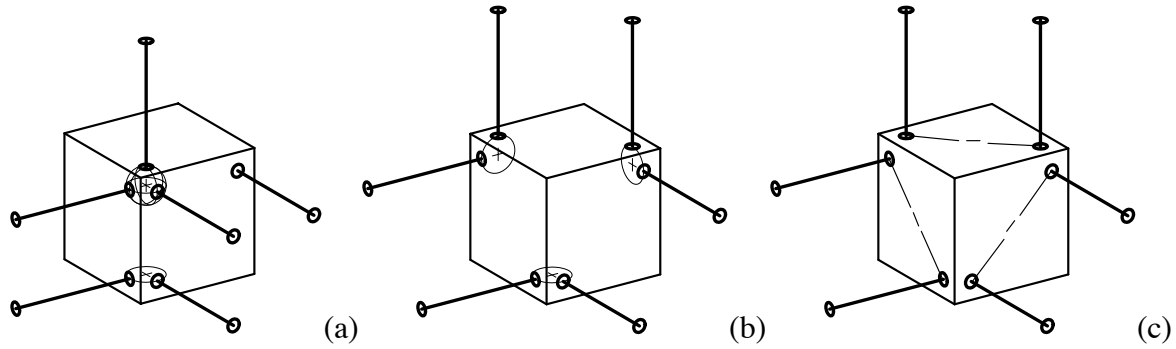

Figure 2-27 In (a), a sphere in a tetrahedral socket provides three constraints; a sphere in a vee provides two constraints; and a sphere on a plane provides the last constraint. In (b), three spheres in three vees each provide two constraints. In (c), three cylinders on three planes each provide two constraints.

The 12 Statements by Blanding are important to understand and to refer to when the time comes to design a constraint system or mechanism. In many cases it is possible to start with a basic design such as one of the familiar kinematic couplings, but as Figure 2-27 shows, any of these can be invented from the orthogonal constraint chart, Figure 2-21, along with a basic understanding of constraint devices such as spheres in vees. Be aware that nice orthogonal constraints and intersecting axes are artificial restrictions used to keep the chart simple and bounded. They should not restrict creativity as many examples in this thesis will demonstrate. Figure 2-28 is such an example of a two-axis gimbal where the rotational axes do not intersect. This design would be appropriate for supporting the principal load along the axis of symmetry such as required for a rocket motor.

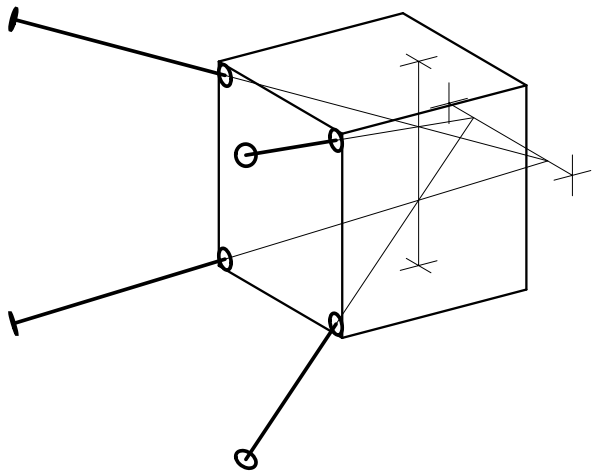

Figure 2-28 Four constraints intersect (and thus allow) two rotational degrees of freedom. The constraints prevent rotation about a third perpendicular axis and translations of those axes. If all four constraints intersected at a point, the result would be an overconstrained, three-axis pivot.

A key concept in exact constraint design is this one-to-one relationship between applied constraints and constrained degrees of freedom. You may choose to add redundant constraints to increase stiffness or to provide a nesting force for contact-type constraints; however, this usually will sacrifice one or more benefits of exact-constraint design. That is to say, the best design may not be the exactly constrained one, but you should begin there so that the implications of overconstraint are fully considered and expected.

2.7 Elastic Averaging

The term elastic averaging describes a condition where two objects are connected through many points of contact in a highly overconstrained manner. Elastic averaging seems so contrary to exact-constraint design that some people may argue one philosophy over the other rather than embracing their complementary virtues. Many kinematic designs rely on bearing systems that function by elastic averaging. A new class of machine tool based on the Stewart platform is a good example [Stewart, 1965-66]. These machines have become know as hexapods because they feature six actuators operating as a parallel-link mechanism to control the relationship between the tool and the workpiece. The actuators typically employ rolling-element bearing technology including ball screws, angular-contact thrust bearings and trunnion bearings. Since many balls share the load, irregularity of any particular ball has little influence over the net error motion. Being massively overconstrained, these devices require very accurate surfaces to fit and function properly, but once achieved, the result is further reduction of error motion due to the averaging of imperfections. Furthermore, the stiffness and load capacity multiply with the number of constraints sharing the load. Rolling-element bearings come in many types and sizes and are relatively inexpensive when mass produced in large quantities.

6 Practical Exact-Constraint Design

The basic concepts of kinematics and exact-constraint design are presented in Section 2.6 following the 12 statements from [Blanding, 1992]. This chapter brings those concepts closer to reality by considering various constraint devices and the many ways that constraints may be arranged. Several analytical studies on flexures provide deeper understanding into the particulars of flexure design. A new approach for kinematic-coupling design optimizes the ability of the coupling to overcome friction and become centered. The approach is most useful for unusual, nonsymmetric configurations where intuition is inadequate. The sometimes complex spatial relationships between constraints, whether for flexures or in couplings, soon become insurmountable unless systematic, matrix-algebra techniques are used to manage all the terms. Working through many such problems has culminated in generalized kinematic modeling software. Written in Mathcad™ Plus 6, programs for flexure systems and kinematic couplings appear in Section 6.3.

6.1 Useful Constraint Devices and Arrangements

Kinematic devices serve many applications that generally require one or more of the following features: 1) separation and repeatable engagement as with a kinematic coupling, 2) defined motion along or about one or more axes, and 3) minimum influence that an imprecise or unstable foundation has on the elastic stability of a precision component. A device is kinematic if it provides the proper number of constraints required for the intended purpose. For example, a supported object should have $n = 6 + f - d$ independent constraints to exactly constrain six rigid-body degrees of freedom plus f flexural degrees of freedom minus d desired axes of motion. In addition to the proper number of constraints, a kinematic design is free of overconstraint.

A purely kinematic design may be difficult (or expensive) to achieve in practice. The term *semi-kinematic* has been used to describe designs that are impure to some extent. That should not imply something is wrong; rather, there are tradeoffs to make in almost every design. It is important to understand the advantages and limitations of various constraint types so tradeoffs can be made to best satisfy the application. I strictly avoid classifying designs as kinematic, semi-kinematic or non-kinematic because there will always be ambiguity. Instead, I advocate applying kinematic design principles within the limits of practical constraint devices; there will almost always be some benefit in doing so. This approach is not limited to precision design but applies to more general machine and mechanism design. See, for example, [Kamm, 1990] and [Reshetov, 1982].

The constraint devices common to precision applications tend to fall into three categories: 1) relatively short-travel flexural bearings (e.g., blade flexures), 2) relatively long-travel bearing components, and 3) repeatable connect-disconnect couplings (e.g.,

kinematic couplings). This chapter focuses on blade flexures and kinematic couplings. Chapter 8, *Anti-Backlash Transmission Design*, presents several common bearing components. See [Slocum, 1992] for more extensive treatment of bearing components.

6.1.1 Basic Blade Flexures

This section presents several common arrangements of blade flexures that provide one axis of motion over a short range of travel. These arrangements: parallel blades, cross blades, and axial blades, are well documented in the literature perhaps with slightly varying names. See, for example, [Jones, 1951, 1962], [Weinstein, 1965], [Siddall, 1970], [Vukobratovich and Richard, 1988] and [Smith, 1998]. A key concept to learn from this section is summarized in the following statement. Several blades connected together as parallel constraints (as opposed to serial constraints) will retain the degrees of freedom that the individual blades have in common. This concept will become clearer after examining the arrangements in this section.

Two parallel blades, connected as shown in Figure 6-1, share a common translational degree of freedom. The rotational degrees of freedom of the individual blades occur about axes that are not in common, thus the combination of two blades constrains those degrees of freedom. Both blades redundantly constrain rotation about the translational axis. A displacement δ_z in the direction of freedom has an associated second-order displacement δ_x given by Equation 6.1. This behavior is a general concern for all flexure designs. All other constraint directions have nominally zero error, although geometric tolerances lead to very small errors that are first order with δ_z.

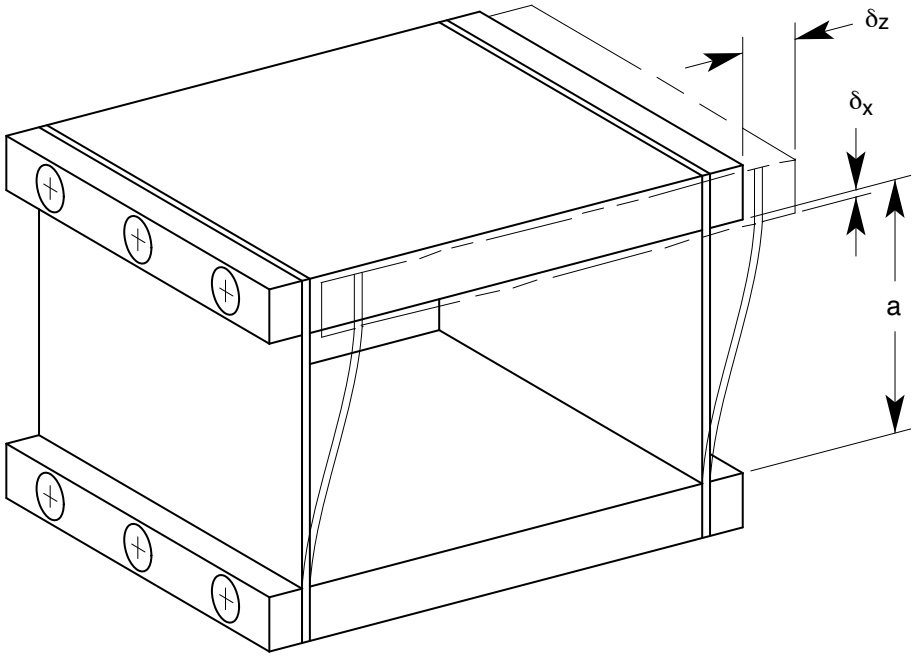

Figure 6-1 Two parallel blades allow one translational degree of freedom and constrain all others. This example shows bolted construction but monolithic designs are also common.

$$\delta_x = \int_0^a \left\{ 1 - \sqrt{1 - \left(\frac{dz}{dx}\right)^2} \right\} dx \cong \int_0^a \frac{1}{2}\left(\frac{dz}{dx}\right)^2 dx = \frac{3\delta_z^2}{5a} \qquad (6.1)$$

Two cross blades, connected as shown in Figure 6-2, share one rotational degree of freedom. One blade constrains the degrees of freedom of the other that are not in common. Both blades redundantly constrain translation along the rotational axis. For a given rotation θ, each blade contributes a second-order radial displacement δ_r given by Equation 6.2. The first term inside the braces is the chord across a deflected blade while the second term is the comparable dimension produced by an ideal hinge. The net result is an extension rather than foreshortening as in parallel blades. The total error is the vector sum from both blades.

$$\delta_r = a\left\{ \frac{2}{\theta}\sin\left(\frac{\theta}{2}\right) - \cos\left(\frac{\theta}{2}\right) \right\} \cong \frac{a\theta^2}{12} \qquad (6.2)$$

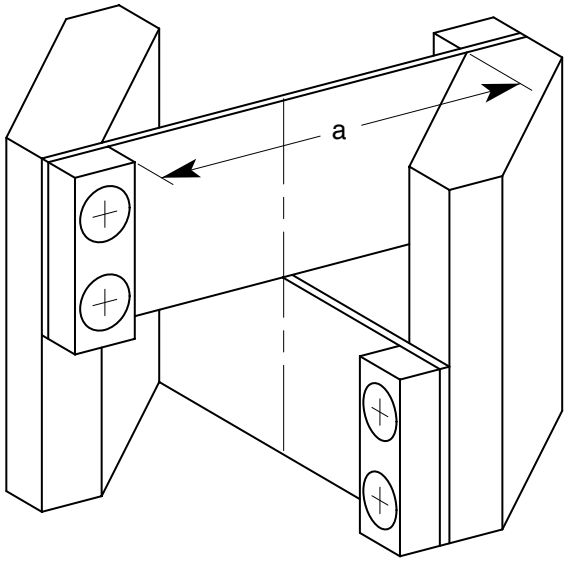

Figure 6-2 Two cross blades allow one rotational degree of freedom and constrain all others. This example shows bolted construction but brazed connections are common in commercial products.

Blades arranged axially, as shown in Figure 6-3, share one rotational degree of freedom. Two blades in different planes are sufficient to constrain the remaining degrees of freedom, but a symmetrical design with four blades is more common. This arrangement has nominally zero radial error motion in contrast to the cross-blade flexure. However, foreshortening of the blades in the axial direction presents an interesting compromise. Equation 6.3 shows the condition required to maintain equal foreshortening across the width of the blades. This condition is satisfied by joining the blades to parabolic-shaped flanges as Figure 6-3 (a) shows. Equation 6.4 shows the condition required to maintain equal bending stress across the width of the blades. The usual compromise solution is to join the blades to conical end caps as Figure 6-3 (b) shows. Making the blades relatively narrow improves this compromise but reduces the stiffness and load capacity of the

flexure. In addition, these equations suggest making the ratio *a/r* large, but they soon become invalid as the geometry diverges from normal beam theory. Finite element analysis is helpful in computing the bending stresses, but a linear code will not represent foreshortening in the blades and the axial stress that may result.

$$\delta_a(r) \cong \frac{3(r\,\theta)^2}{5a} \quad \rightarrow \quad a \propto r^2 \tag{6.3}$$

$$\sigma_b(r) \cong \frac{3E\,t(r\,\theta)}{a^2} \quad \rightarrow \quad a^2 \propto r \tag{6.4}$$

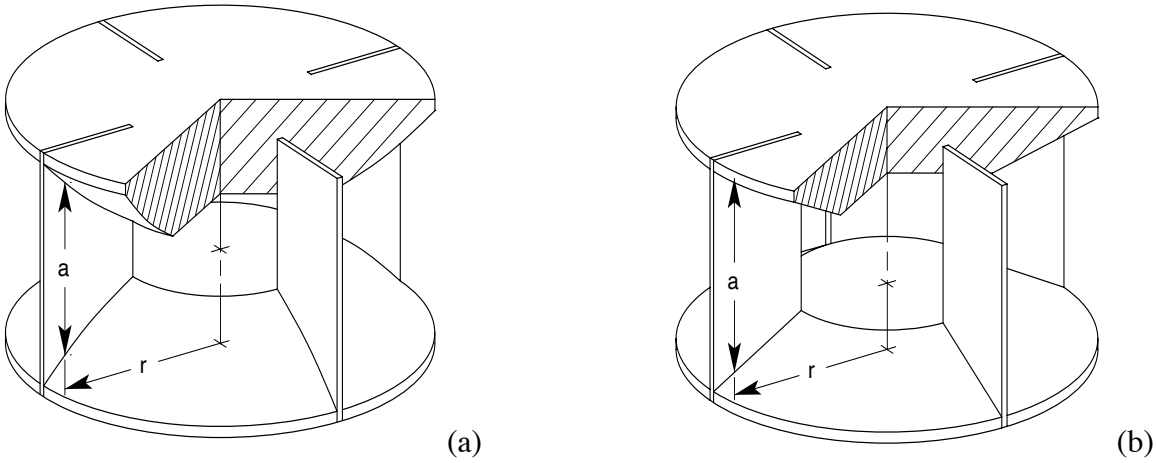

Figure 6-3 Axial blades allow one rotational degree of freedom and constrain all others. The shape of the flanges is important to the behavior of the flexure. In (a), two paraboloids that share a common vertex satisfy equal axial displacement across the blades. In (b), two cones that share a common vertex provide a reasonable compromise between equal axial displacement and equal bending stress across the blades.

6.1.2 Basic Kinematic Couplings

A kinematic coupling provides rigid and repeatable connection between two objects through usually six local contact areas. This is the case for the two traditional configurations shown in Figure 6-4: (a) the three-vee coupling and (b) the tetrahedron-vee-flat coupling (also known as the Kelvin clamp). The weight of the object being supported or some other consistent nesting force holds the surfaces in contact. A spring or compliant actuator may apply the nesting force, but ideally it should allow all surfaces to engage freely with minimum friction and wear. Otherwise, the coupling will not become *centered* as precisely as it should or perhaps not at all. Friction between the contacting surfaces acting on the compliance of the coupling is a main contributor to nonrepeatability as experimentally determined by [Slocum and Donmez, 1988].

The symmetry of three vees offers several advantages: better distribution of contact forces, better centering ability, thermal expansion about a central point and reduced manufacturing costs due to identical features. Conversely, the tetrahedral socket offers a

natural pivot point for angular adjustments. Many tip-tilt mirror mounts operate in this fashion. The three-vee coupling is the natural choice for adjustments in six degrees of freedom or when there is no need for adjustment.

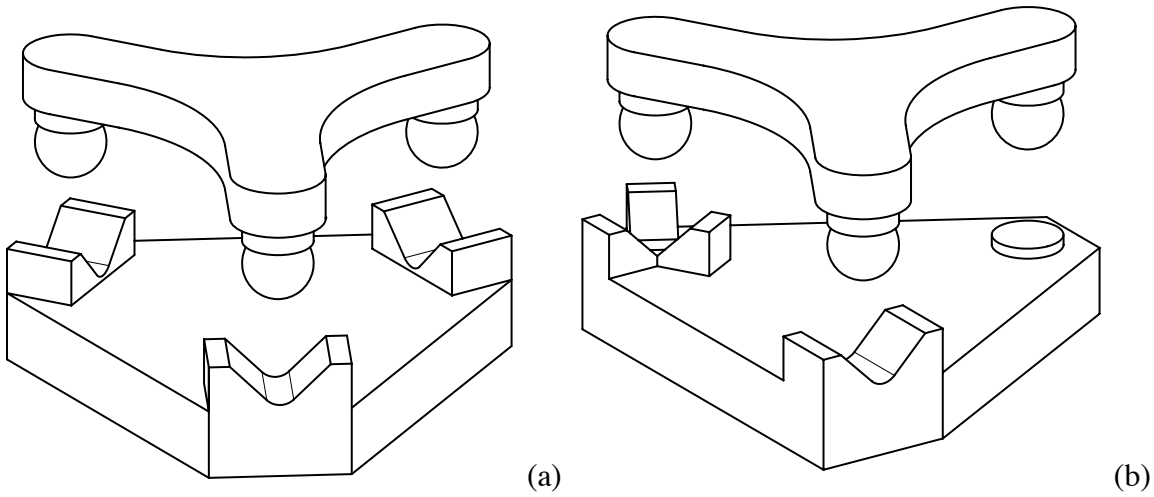

Figure 6-4 In (a), the three-vee coupling has six constraints arranged in three pairs. In (b), the tetrahedron-vee-flat coupling has six constraints arranged in a 3-2-1 configuration. Often for manufacturing reasons, the tetrahedron is replaced with a conical socket, hence the more familiar name cone-vee-flat.

The local contact areas of the traditional kinematic couplings are quite small and require a Hertzian analysis to ensure a robust design for the chosen material pair (see Appendix C, *Contact Analysis*). Greater durability is achieved by better curvature matching between contacting surfaces. Rather than use a full sphere against a flat surface, a partial sphere of much larger radius may be used instead. The same applies to cylindrical surfaces contacting with crossed axes. Another approach is to use a full sphere against a concave spherical or cylindrical surface. Figure 6-5 compares these two approaches for a vee constraint. Both constraints have the same relative (or effective) radius but the sphere in a gothic arch has less capture range.

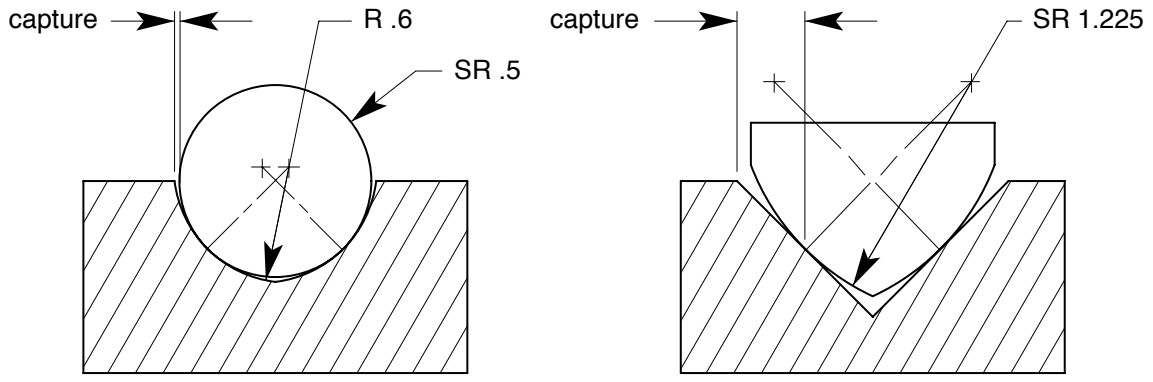

Figure 6-5 A vee constraint showing two ways to increase the area of contact. Capture is the maximum distance off center that the constraint will engage with tangency.

Designs based on line contact rather than point contact offer a significant increase in load capability and stiffness. For example, line contact forms between a precisely made, heavily loaded sphere and conical socket. The kinematic equivalent to three vees is a set of three sphere-cone constraints with either the spheres or the cones supported on radial-motion flexures. The upper member in Figure 6-6 (a) has six rigid-body plus three flexural degrees of freedom that three cones exactly constrain. Alternatively in (b), the three-tooth coupling forms three theoretical lines of contact between cylindrical teeth on one member and flat teeth on the other member. Each line constrains two degrees of freedom giving a total of six constraints. Manufactured with three identical cuts directly into each member, the teeth must be straight along the lines of contact but other tolerances may be relatively loose. Both of these kinematic couplings are being used on the EUVL project to overcome the limited hardness of super invar.

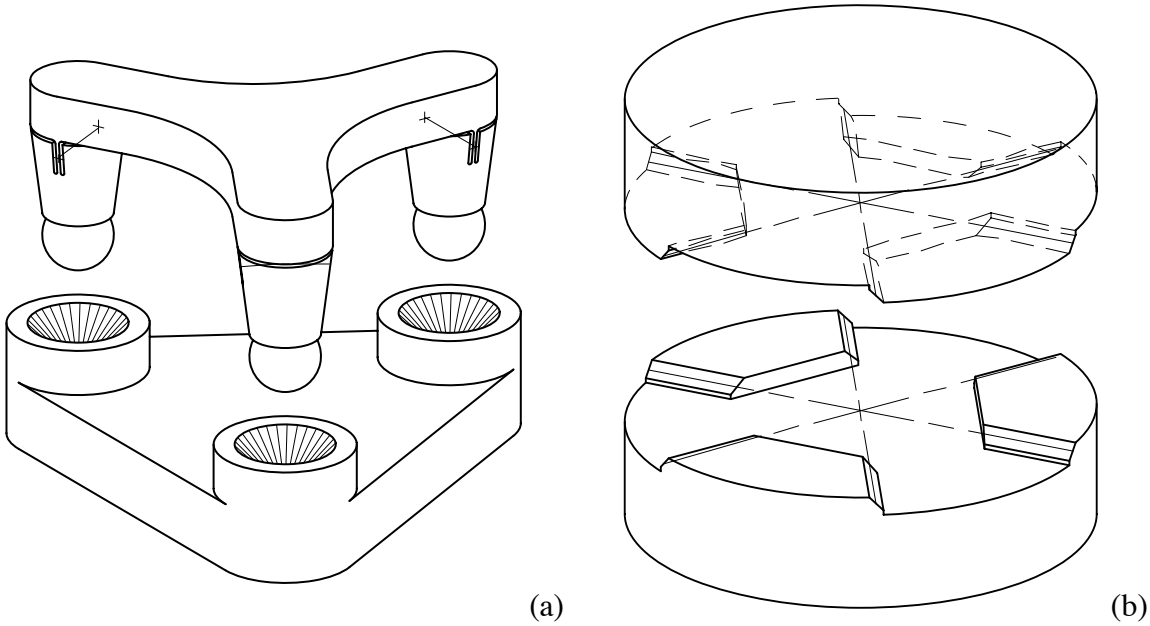

Figure 6-6 In (a), flexure cuts in the upper member allow each sphere limited radial freedom to seat in the conical sockets of the lower member. In (b), the three-tooth coupling forms three theoretical line contacts between cylindrical teeth on one member and flat teeth on the other member.

6.1.3 Extensions of Basic Types

Arranging constraints is a design process that requires a basic understanding of kinematics and the mechanics of constraint devices. The blade flexures and kinematic couplings presented thus far are good examples from which to learn and start new designs. This section presents several interesting and useful extensions based on three vee constraints. The examples range from fairly direct implementation on a touch trigger probe to a less obvious flexure stage with three degrees of freedom. In my experience, thinking of six constraints as three pairs has been a valuable and simplifying conceptual construct.

6.1.3.1 Touch Trigger Probe

Touch trigger probes are commonly used on coordinate measuring machines to indicate precisely where in the travel of the machine axes that contact is made with the workpiece. It is sufficient if the probe signal occurs with a known position lag as this is easy to correct in software. A common design studied by [Estler, et al., 1996, 1997] employs a three-vee kinematic coupling that acts as the electrical switch and the mechanical registration. The problem that Estler addresses through modeling and compensation is the variation in position lag depending upon the direction of travel, the orientation of the surface and other effects. A dominant error term, referred to as probe lobing, results from a three-fold variation in the trigger force acting on the compliance of the probe shaft.

The heart of the problem is the orientation of the vee constraints. Figure 6-7 shows the probe mechanism studied by Estler (a) and a new design (b) that solves probe lobing, at least in theory. In (a), the probe side of the coupling is preloaded down by a compression spring into three vee constraints represented by angled cylinders. The probe will not trigger until there is sufficient moment imparted to the coupling for any of the constraints to become unloaded, thus breaking electrical continuity. Although the preload is constant, the lever arm may vary up to a factor of two depending whether the coupling pivots about one vee or two. In (b), the new vee orientation requires a torsional preload to seat the coupling. In addition, the spring would be set to off-load the weight of the probe coupling. In this configuration, any applied moment (orthogonal to the preload) equally unloads one side of each vee; there is no directional preference. The downside will be a greater influence of friction since any pin must now slide up or down a vee rather than simply lifting out.

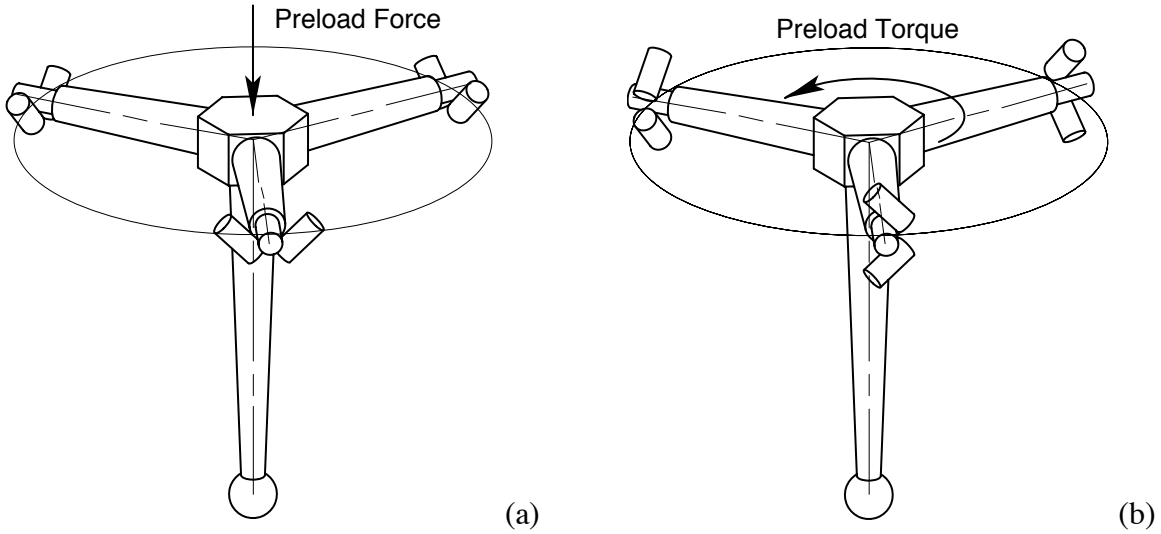

Figure 6-7 In (a), the moment required to unseat one vee while pivoting about the other two vees is a factor of two less than the moment required to unseat two vees while pivoting about the third vee. In (b), a moment applied about any axis in the plane of the vees produces equal reaction at all vees.

6.1.3.2 The NIF Diagnostic Inserter

The NIF requires a number of diagnostic instruments near the center of the 10 m diameter target chamber. Each instrument is transported approximately 6 m into the chamber by a telescoping diagnostic inserter. Since only the end position of travel requires submillimeter positioning, a kinematic coupling is being considered to provide repeatable registration at the end of a rather imprecise telescoping stage. However, the long, skinny geometry of the inserter presents an unfavorable aspect ratio for a traditional kinematic coupling. The configuration shown in Figure 6-8 was proposed to work within the geometric constraints yet provide acceptable moment stiffness and capacity. It was conceived by splitting the vees of a three-vee coupling and axially separating the odd-numbered constraints from the even-numbered constraints. The odd-numbered constraints act like a right-hand screw while the even-numbered constraints act like a left-hand screw. An applied axial preload force translates the cylinder until all constraints are engaged and an axial torque is established between the two sets of three constraints.

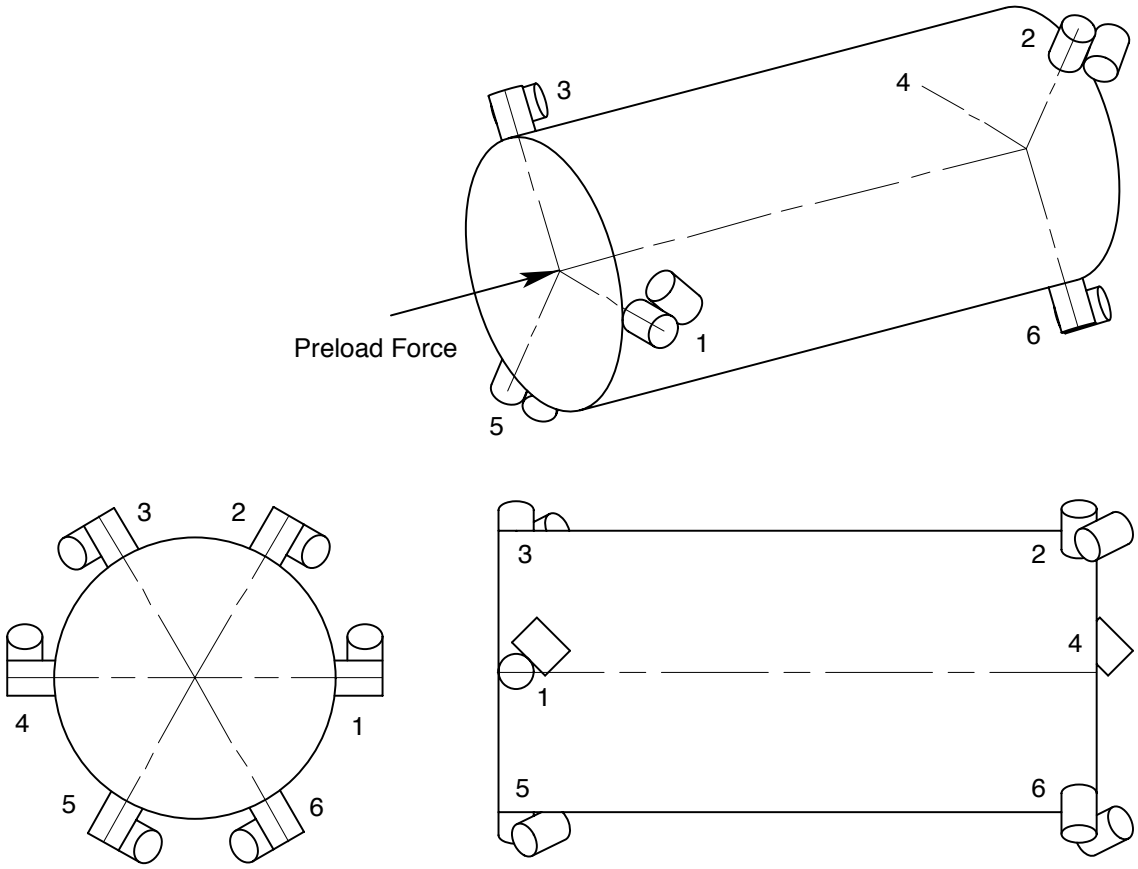

Figure 6-8 The end view looks much like a three-vee coupling with constraint pairs 2-3, 4-5 and 6-1 apparently forming three vees. The side view shows the significant separation between odd- and even-numbered constraints. As in Figure 6-7, the angled cylinders are constraints fixed to an unseen structure.

6.1.3.3 The NIF optics assembly

The NIF requires many hundreds of kinematic couplings to support large, replaceable optics assemblies. There are several types of kinematic couplings used throughout the system, but one in particular demonstrates a simple evolution from a basic three-vee coupling to a more novel configuration well suited for tall assemblies. Figure 6-9 shows the evolution in three simple steps. The horizontal configuration is convenient because gravity provides the preload. Rotating the coupling to the vertical configuration has obvious consequences, which motivates the next step to rotate the lower vees to carry the gravity load. It is important that the centroid of the supported object be offset from the lower vees in a direction that preloads the upper vee. The next step of spreading the upper vee has a particular advantage for NIF optics assemblies. The widely spaced vee provides frictional constraint that stiffens the torsional vibration mode of the optics assembly. This example appears again in Section 6.3.3 and Chapter 7.

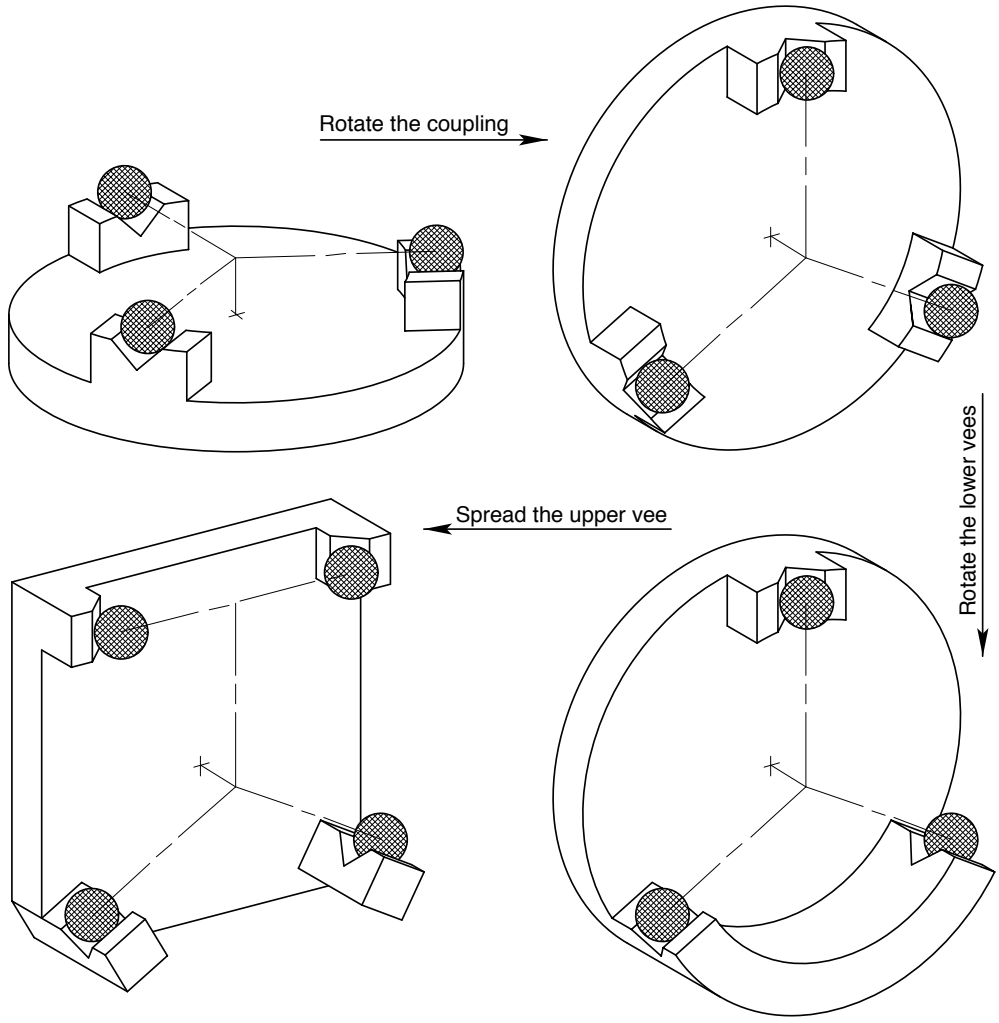

Figure 6-9 The evolution from a horizontal three-vee coupling to the configuration used for many NIF optics assemblies. The spheres in each configuration attach to the object being supported.

6.1.3.4 EUVL Mirror Mount

Friction between the contacting surfaces of a kinematic coupling is a disadvantage when it causes significant distortion in the precision component being supported. A common approach for mounting super-precision optics is an arrangement of three vee-flexures that [Vukobratovich and Richard, 1988] refer to as bipods. Figure 6-10 shows the bipod design used for EUVL mirror mounts. Each leg consists of four blades in series to provide one constraint and five degrees of freedom. One bipod provides the same constraint as a sphere and vee but without friction. Three bipods fully constrain the supported object with six constraints connected in parallel. Notice too that the top of the bipod has the features for a three-tooth coupling. There are mating features on the optic to provide the connect-disconnect function. The kinematic repeatability of the couplings ensure repeatable forces imposed by the bipod flexures on the optic, leading to a repeatable distortion between optic manufacturing and final use. This example appears again in Chapter 7 in greater detail.

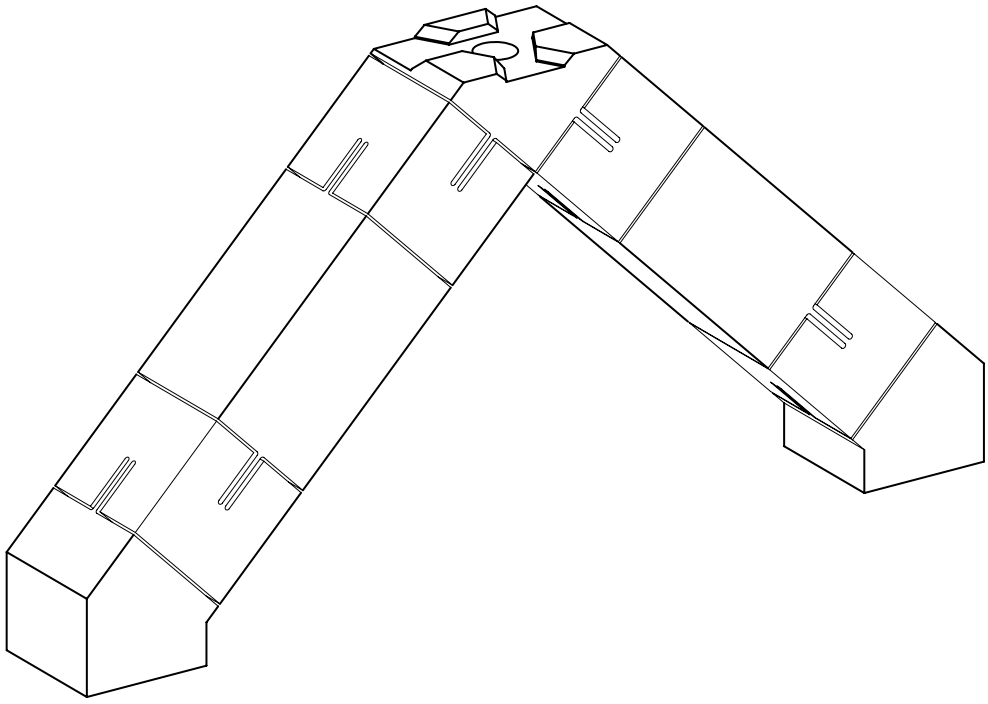

Figure 6-10 A single bipod flexure constrains two degrees of freedom in the plane of the vee. Usually the center section connects to the precision component and the ends connect to the support. At times it may be advantageous to reverse this role for better weight distribution provide by six supports.

6.1.3.5 X-Y-θ_z Flexure Stage

A flexure stage that provides pure planar motion (X-Y-θ_z) satisfies a number of applications found particularly in microelectronics and opto-mechanical systems. One approach to this problem is to serially connect single-axis flexure stages, for example, two sets of parallel blades and one set of cross blades. Besides being an awkward design, good stiffness in each constraint direction is difficult to obtain. When possible, it is better to

arrange constraints in parallel. An obvious example is a set of three single-constraint flexures arranged physically parallel to each other. This arrangement is rigid and simple, but has second-order, out-of-plane error motion that can only be reduced with longer constraints. A better arrangement appears in Figure 6-11. It consists of three folded-hinge flexures arranged as parallel constraints. This arrangement provides pure planar motion except for errors arising from geometric tolerances.

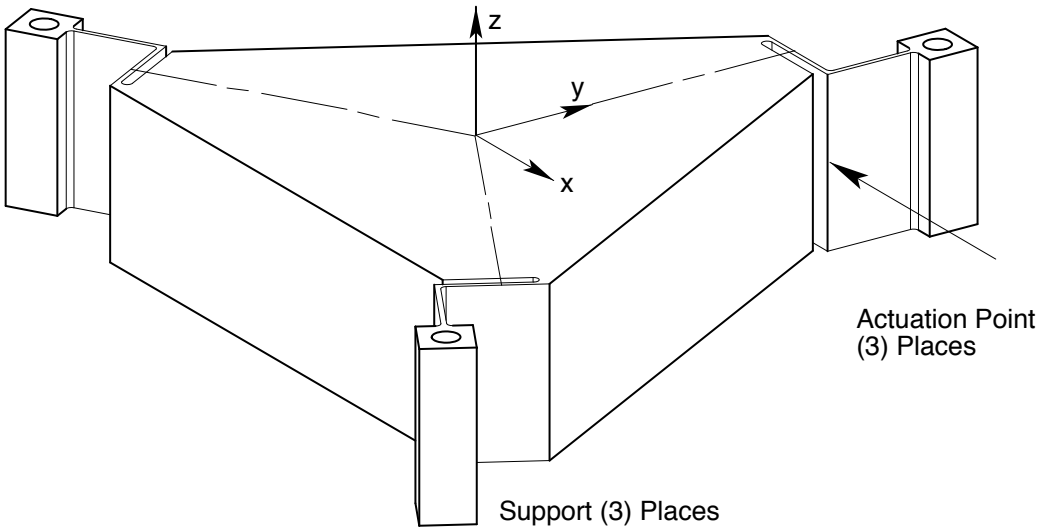

Figure 6-11 Three folded hinge flexures constrain motion within a plane and provide convenient points with which to actuate the stage.

The folded hinge provides one constraint although it appears compliant in all directions. Rather, the two blades have one degree of freedom in common so only five of the six (2 x 3 DOF) are independent. One nice feature of the folded hinge is the convenient point to apply actuation, for example, with a micropositioner. This was the approach used for an EUVL X-Y stage that appears in Chapter 7. [Ryu, Gweon and Moon, 1997] designed an X-Y-θ_z wafer stage that uses piezoelectric actuators driving folded hinges.

6.2 Analytical Design of Flexures

Much has been written about the analysis of flexures, so much so that the papers are seemingly saturated with the same information. There has been little new understanding presented in resent years. The emphasis in this section is in providing new information and understanding. This is accomplished using both beam theory and finite element analysis. A fundamental contribution is a matrix-algebra technique for modeling flexure systems. The equations for a blade flexure are contained in a compliance matrix and a stress matrix, both of which consider column effects. This is a sophistication not found in the formulas of Section 2.6. Computer software written for specific configurations such as the bipod flexure has proved very valuable in the case studies for this thesis. A general-configuration program for flexure systems, written in Mathcad™ Plus 6, appears in Section 6.3.

6.2.1 Comparison of Flexure Profiles

The blade flexures presented thus far have had constant thickness except perhaps near the ends where small fillets are typical. Another common flexure profile is the circular hinge, which typically is manufactured by drilling two adjacent holes to form the flexure and then by relieving other material as necessary to allow freedom of motion. The primary reference for the circular hinge is [Paros and Weisbord, 1965]. More recently, the elliptical hinge was studied by [Xu and King, 1996] and [Smith et al., 1997]. When the thickness of the flexure is small compared to the circle or ellipse, both of these profiles are well approximated by a parabola. A parabolic profile leads to simpler equations and better understanding. Since these three profiles have effectively the same performance, the circular hinge is the obvious choice for ease of manufacturing (whether by drilling holes or using circular interpolation). The interesting comparison is between the (circular, elliptical or parabolic) hinge flexure and the blade flexure because each has particular advantages.

To remain the most general, the presentation uses the elliptical profile described by the major and minor diameters a and b, respectively. For a circular profile, simply replace both a and b with the diameter d. Equation 6.5 gives the thickness profile for the ellipse and its approximate parabolic profile. Figure 6-12 compares these two profiles for an example that is near the limit for a good approximation. The approximation is better for a circular profile and of course when the minimum thickness t_0 is thinner. The straight lines in the figure have to do with the comparison to the equivalent blade flexure discussed later.

$$t_e = t_0 + b\left[1 - \sqrt{1 - \left(\frac{2x}{a}\right)^2}\right] \cong t_0 + \frac{b}{2}\left(\frac{2x}{a}\right)^2 = t_p \qquad (6.5)$$

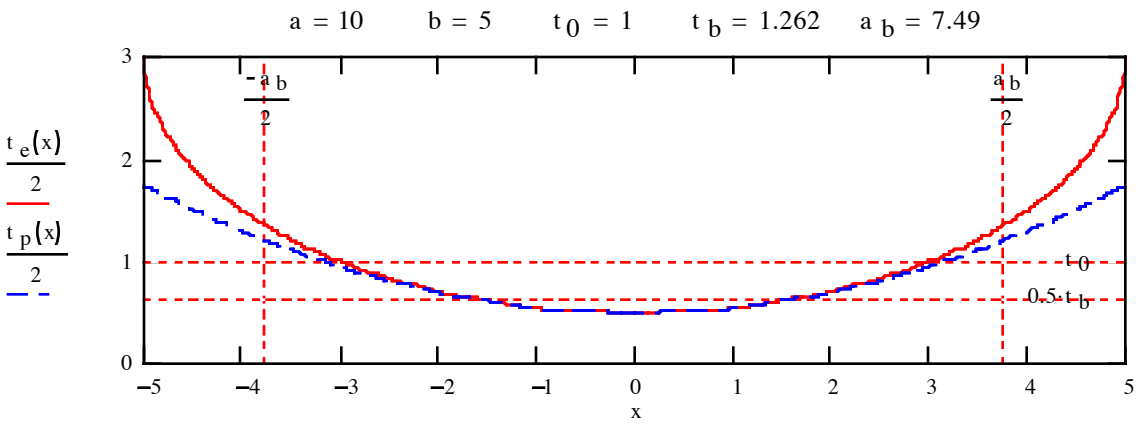

Figure 6-12 The solid line indicates the profile for one side of an elliptical hinge flexure. The horizontal axis is a plane of symmetry. The parabola (dash line) provides a good approximation in the thin region of the flexure that governs both the axial and moment compliance. The equivalent blade flexure is bounded by straight lines indicated by a_b and t_b.

Equations 6.6 and 6.7 give simplified expressions for axial compliance and moment compliance, respectively, for the parabolic profile. For this example, the axial compliance

of the ellipse is underestimated by 3% and the moment compliance is overestimated by 5% compared to *exact* solutions using the elliptical profile. However, the use of beam theory in the derivation is itself an approximation. These solutions are similar to those for the blade flexure. If the blade were taken to be of length a and thickness t_0, then the term in square brackets would represent the factor by which the hinge flexure was different.

$$c_x = \frac{1}{E\,w}\int_{-a/2}^{a/2} t_p^{-1}\,\mathrm{d}\,x \cong \frac{a}{E\,w\,t_0}\left[\frac{\pi}{2}\sqrt{\frac{2t_0}{b}} - \frac{2t_0}{b}\right] \tag{6.6}$$

$$c_\theta = \left(1-\nu^2\right)\frac{12}{E\,w}\int_{-a/2}^{a/2} t_p^{-3}\,\mathrm{d}\,x \cong \left(1-\nu^2\right)\frac{12\,a}{E\,w\,{t_0}^3}\left[\frac{3\pi}{16}\sqrt{\frac{2t_0}{b}}\right] \tag{6.7}$$

It is instructive to consider the length and thickness of a blade that is equivalent to the hinge flexure in terms of axial and bending compliance. The solution to two equations with two unknowns appears in Equation 6.8, where the subscript b indicates the equivalent blade parameters. This explains the straight lines in the figure marked with either a_b or t_b. The line marked t_0 indicates the part of the parabola that has the greatest slenderness ratio for buckling. The usual definition for slenderness ratio is the length divided by the minimum radius of gyration. Here it is more convenient to use the length divided by the thickness. It is obvious from the figure that the equivalent blade being both longer and thinner is more likely to buckle under a compressive load. Equation 6.9 gives the condition required for the hinge flexure to yield before buckling and the factor by which the equivalent blade flexure is more likely to buckle. For this example the factor is 1.88.

$$\frac{a_b}{a} \cong \sqrt{\frac{16}{3\pi}\frac{2t_0}{b}\left[\frac{\pi}{2} - \sqrt{\frac{2t_0}{b}}\right]^3} \qquad \frac{t_b}{t_0} \cong \sqrt{\frac{16}{3\pi}\left[\frac{\pi}{2} - \sqrt{\frac{2t_0}{b}}\right]} \tag{6.8}$$

$$SR_p \cong \frac{a}{\sqrt{2t_0\,b}} < \pi\sqrt{\frac{E}{12\sigma_y}} \qquad \frac{SR_b}{SR_p} \cong \pi - 2\sqrt{\frac{2t_0}{b}} \tag{6.9}$$

The hinge flexure clearly has the advantage over the blade flexure for buckling resistance. The bending stress appears to be slightly higher for the thinner hinge flexure, since both equivalently require the same bending moment for a given rotation, but stress concentrations in the fillets of the blades can be just as high. The main advantage for the blade flexure comes when there is need for rotational flexibility about the axis of the blade, so as to twist. Of course the hinge flexure is better if the application calls for resisting twist. This is also true if the flexure is to be used as a secondary constraint in shear.

6.2.2 A Study on Fillets for Blade Flexures

Beam theory works well for blade flexures except at each end where there is a transition to some larger cross section. Monolithic blade flexures are usually manufactured with small corner radii know as fillets. Clamped blades, on the other hand, usually have very abrupt transitions that are difficult to model with any certainty. The edges of the clamping surfaces may have partial radii to transition the clamping force, but it is assumed that microslip will relieve the theoretically high stress concentration for axial and moment loads. Naturally the subject of this study is the behavior of fillets as a function of radius size. This is accomplished through a parameterized finite element model for one end of the blade.[I] In the study, the radius varies from one-half blade thickness to twice the blade thickness, and the model is subject to either axial or moment loading. Curve fits to the finite-element results are useful to supplement the limitations of beam theory.

An assumption is made in beam theory that either the out-of-plane stress or the out-of-plane strain is zero. The same is true for 2D FEA. The two choices bracket the range of a 3D model, plane stress for zero width and plane strain for infinite width. Both types were compared to a 3D model of varying widths. Consistent with the general practice in flexure design, plane stress is most appropriate in the calculation of axial stiffness and stress due to axial and moment loads. However, the results indicate that plane strain is more appropriate for moment stiffness, contrary to general practice. The effect is rather small, only 5 to 10 percent but in the nonconservative direction. Hence, the equations found in this thesis for bending of flexures have a factor $(1 - \nu^2)$ to account for stiffening due to the Poisson effect.[II] The same is true for the finite-element results that appear later in this section.

The shape of the transition region and the range of fillet radii are apparent in Figure 6-13. In this case, an axial load is applied to the left end of the 20 x 20 block, and the right end of the 2 x 10 blade is constrained. In Figure 6-14, opposite forces on the top and bottom of the block generate a moment load. Both figures show the deflected shape of the model and contours of von Mises stress. Although difficult to see, the maximum stress for axial loading occurs approximately at the quarter point of the fillet closest to the blade and occurs very near the start of the fillet for moment loading. The node on the lower right corner of the block is the displacement location used for the compliance calculations. All the results presented are normalized to the blade thickness *t* and calculations from beam theory.

[I] Pro/MECHANICA by Parametric Technology Corp. is the finite element software used in this study.

[II] The bending stress across the thickness of the flexure changes from tension to compression over a very short distance. The blade would bow if not connected on each end to a stiff structure. The plane-strain assumption does not allow any bowing so the calculation underestimates the desired quantity, bending compliance. The blade has some opportunity to bulge in width when axially loaded. The plane-stress assumption freely allows bulging so the calculation underestimates the desired quantity, axial stiffness. The maximum stress due to axial and moment loads occurs on the sides where the plane-stress assumption is valid.

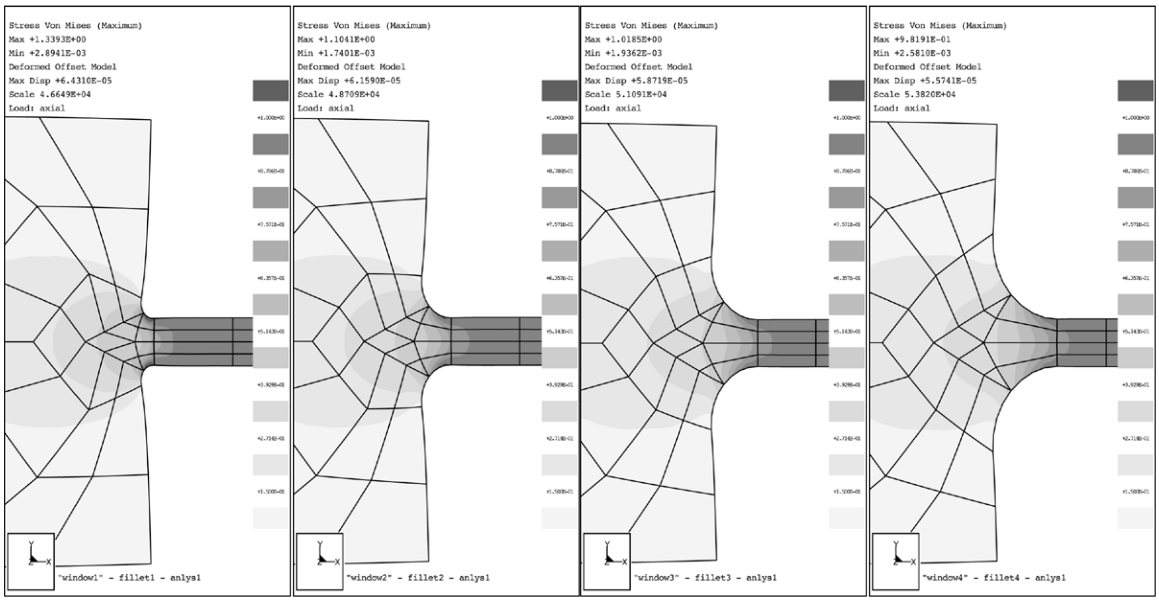

Figure 6-13 The fillet radii shown here are one-half, one, three-halves and two times the blade thickness. The deflected shape and the contours of von Mises stress result from an axial load.

Figure 6-14 The fillet radii shown here are one-half, one, three-halves and two times the blade thickness. The deflected shape and the contours of von Mises stress result from a moment load.

The maximum stress from the 2D plane-stress model divided by the stress calculated from beam theory is the stress concentration factor plotted in Figure 6-15 for axial loading and Figure 6-16 for moment loading. In each graph, the solid line is a fitted curve to discrete results from the finite element model. The equation at the top of each graph may be used to calculate the stress concentration factor for any radius-to-thickness ratio between one-half and two. The knee in the curve appears to be at a ratio near one.

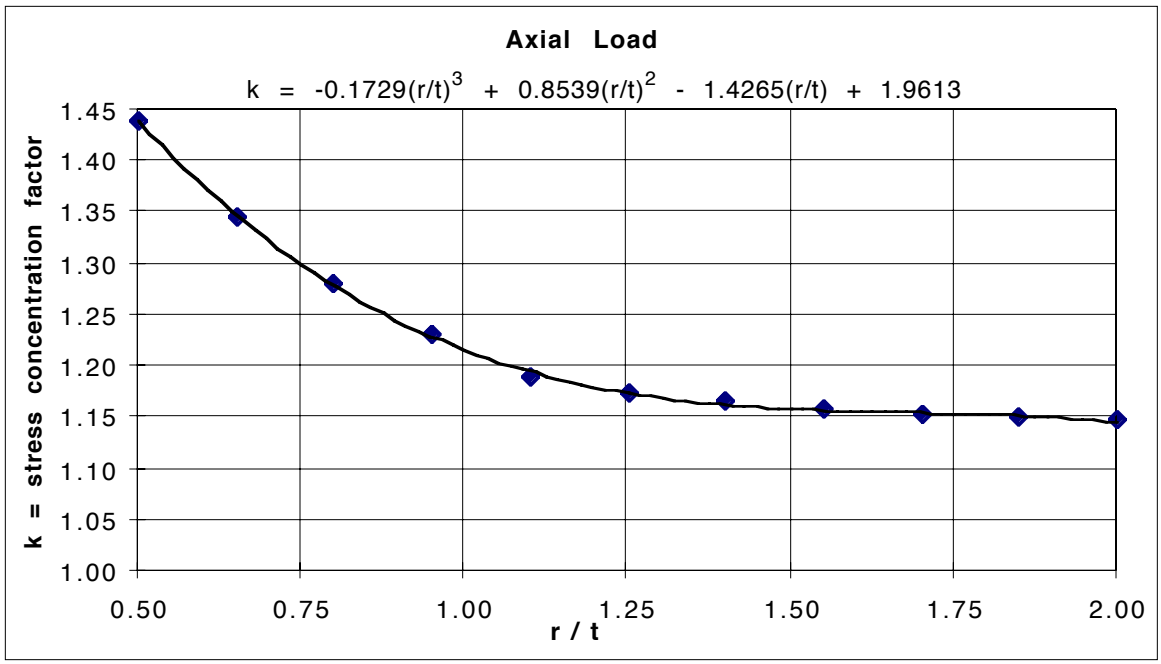

Figure 6-15 The stress concentration factor for axial loading is closely approximated by a cubic polynomial, where *r/t* is the ratio of fillet radius to blade thickness.

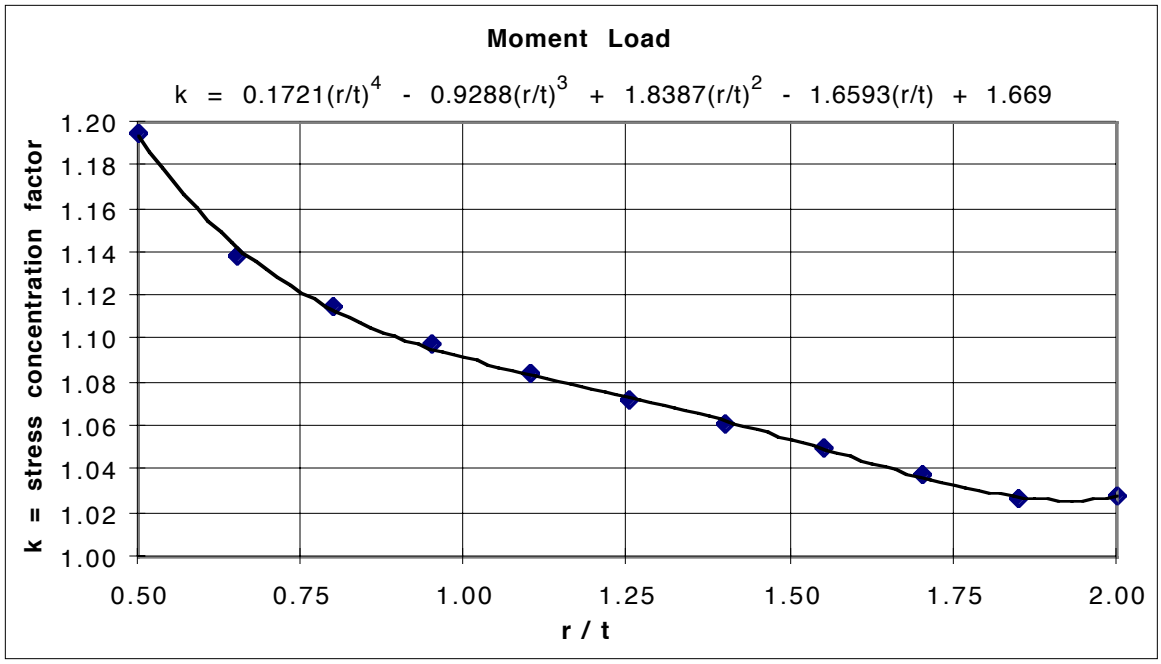

Figure 6-16 The stress concentration factor for moment loading is closely approximated by a fourth-order polynomial, where *r/t* is the ratio of fillet radius to blade thickness.

The size of the fillet radius also has an effect on the amount of deflection under load. A larger fillet shortens the effective length of the blade assuming that the end structures remain separated by a constant distance *a*. This effect on blade length is apparent in Figure 6-17 for axial loading and Figure 6-18 for moment loading. The curves give the

additional length of blade required to make beam theory match the displacement predicted from the finite element model. As might be expected, the compliance due to the elasticity of the end structures is significant for axial loading. For moment loading, beam theory matches the finite element model for a ratio $r/t = 0.62$.

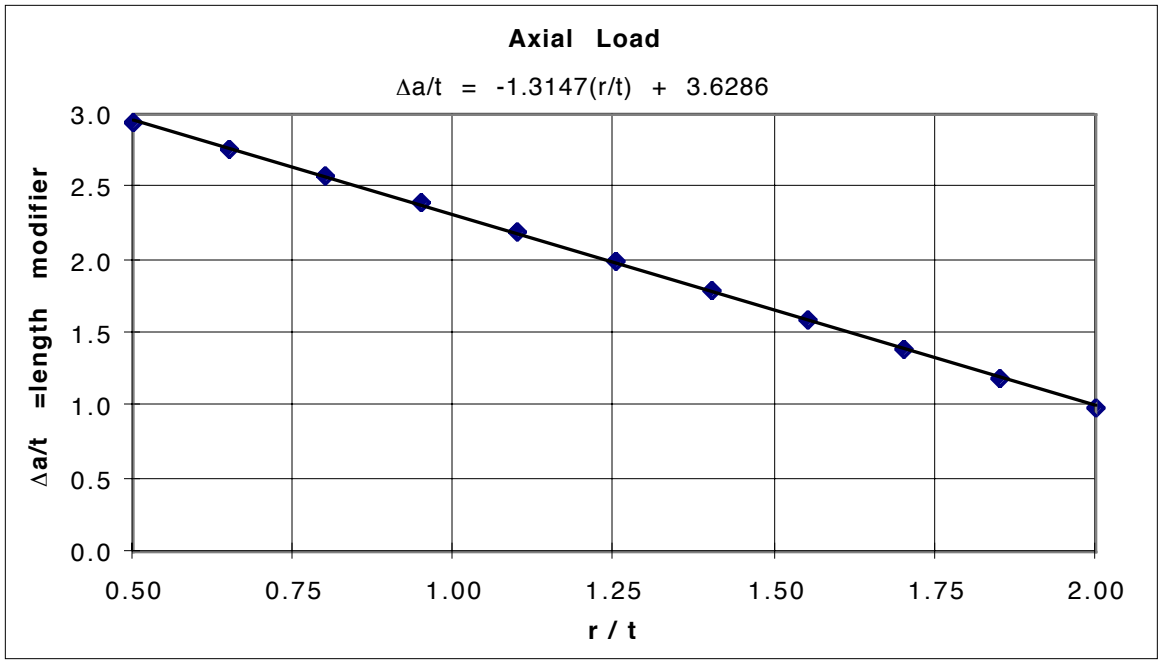

Figure 6-17 The length modifier for axial loading is closely approximated by a linear curve, where *r/t* is the ratio of fillet radius to blade thickness.

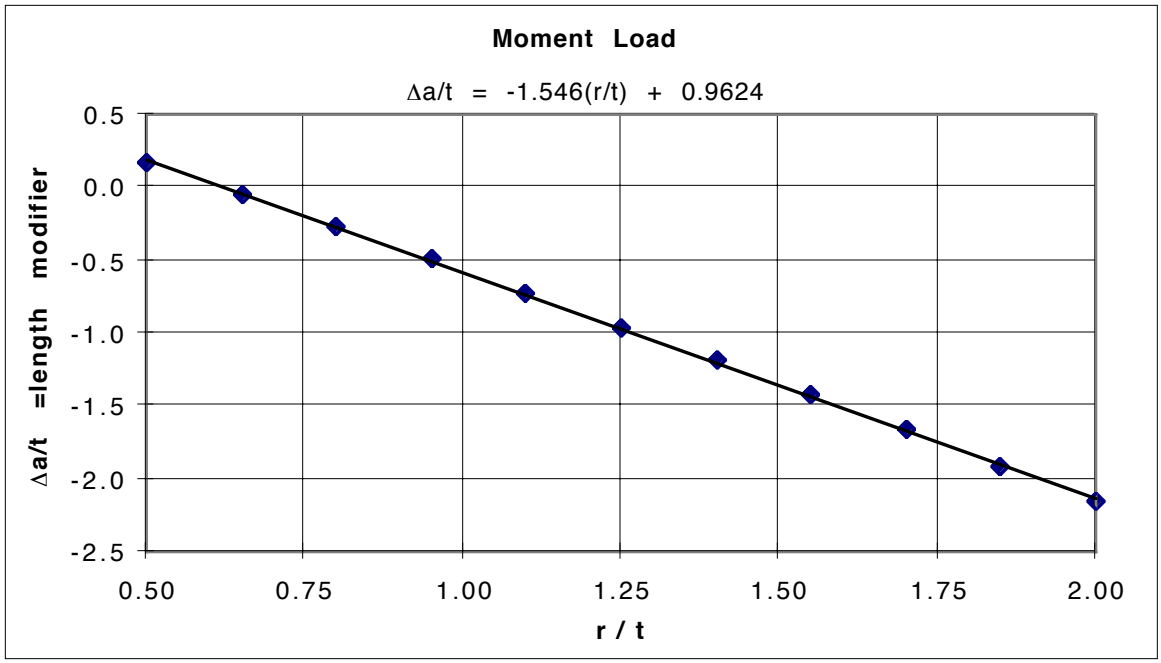

Figure 6-18 The length modifier for moment loading is closely approximated by a linear curve, where *r/t* is the ratio of fillet radius to blade thickness.

6.2.3 The Compact Pivot Flexure

An axial arrangement of two blades in series is a useful single-constraint device that provides angular freedom about three axes. Since the two translational degrees of freedom are rather stiff for short blades, it is common to duplicate another set of two blades some distance along the axial constraint direction. See, for example, the bipod flexure in Figure 6-16. The same cuts used to make the bipod flexure appear more clearly in Figure 6-19 (a). This basic design is being used on the NIF and EUVL projects. An advantage of this design becomes apparent when compared to the more common design in (b), where the axial compliance introduced at the junction between blades is significant. It clearly shows the compromise between axial stiffness and how closely spaced the blades can be. The design shown in (a), with much deeper end sections, greatly relieves this compromise. Even so, it starts to become an issue again when the blade is wider than four times its length. This three-dimensional behavior is best studied with 3D finite element analysis. As before, finite-element results are displayed so as to extend the usefulness of simple theory.

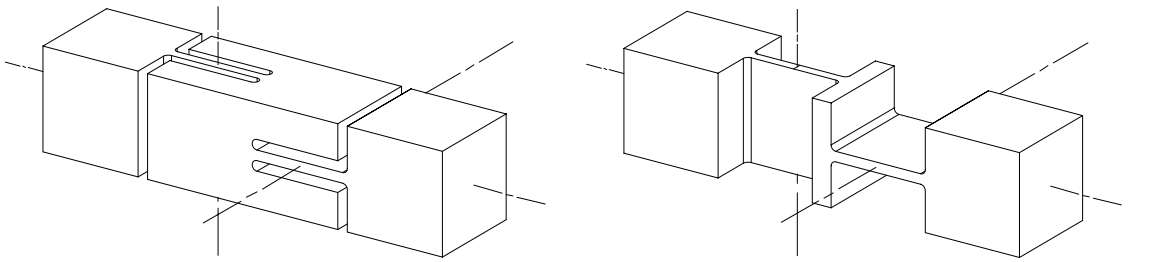

(a) (b)

Figure 6-19 The design in (a) allows the minimum spacing of blades and maintains good axial stiffness. In addition, the gaps may be controlled to provide over-flexion protection. In order for the design in (b) to have good axial stiffness, the junction between blades would have to be lengthened.

Since only axial displacement is of interest in this study, the use of symmetry boundary conditions at two midplanes simplifies the model to just one-quarter the physical pivot flexure. This model, shown in Figure 6-20, also aids in viewing contours of von Mises stress through the blades. The variable parameter in this study is the blade width w, which varies from one to four times the length a. The blade length is ten times the thickness and the fillet radius is one-half the blade thickness.

Although the blades become stiffer with increasing width, the aspect ratio of the junction becomes less favorable and contributes a larger proportion to the total compliance. This is the reason in Figure 6-21 that the axial displacement when normalized to theory increases with blade width. This behavior is also apparent in von Mises stress as gradients that increase with blade width. Figure 6-22 shows how stress varies across the half-width taken through the center of the blade (length and thickness). Figure 6-23 shows how stress varies along the axis of symmetry. Notice that these stresses are away from the stress concentrations caused by fillets. A practical maximum for blade width is two times the length partly because the torsional stiffness increases rapidly with the ratio w/a.

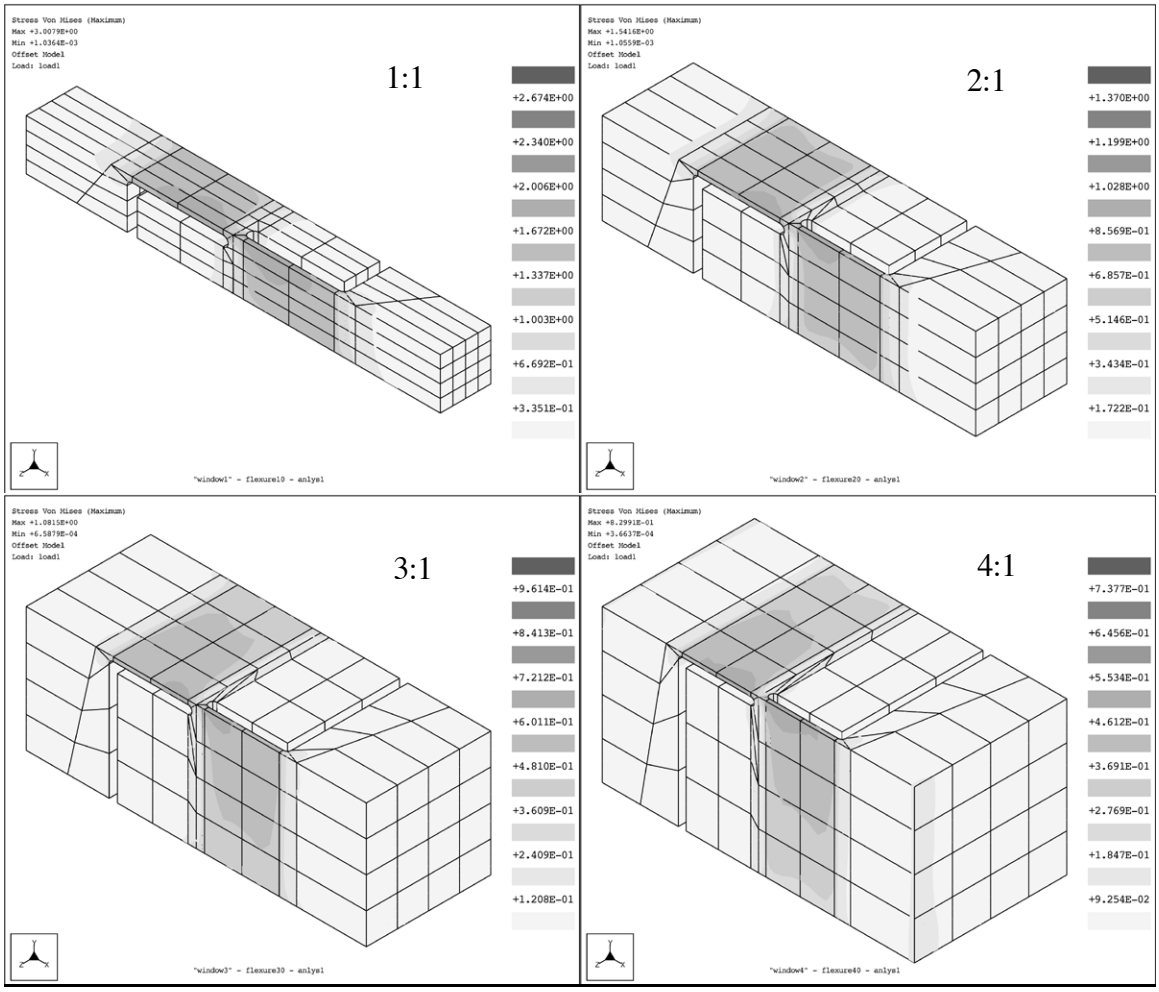

Figure 6-20 Contours of von Mises stress for blade widths from one to four times the blade length.

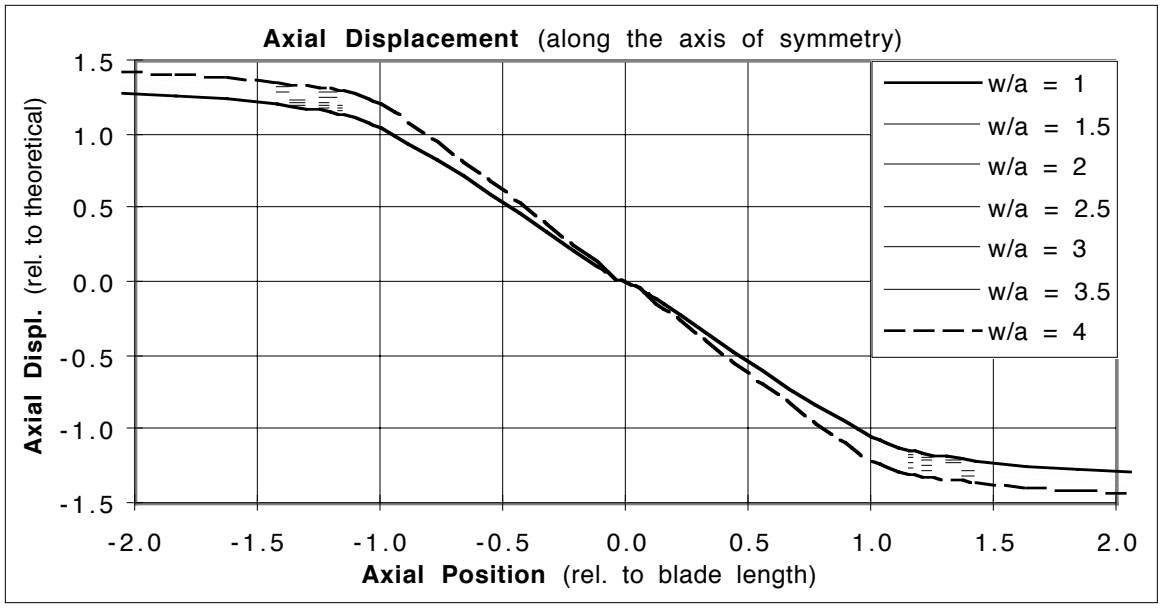

Figure 6-21 Axial displacement versus axial position along the axis of symmetry.

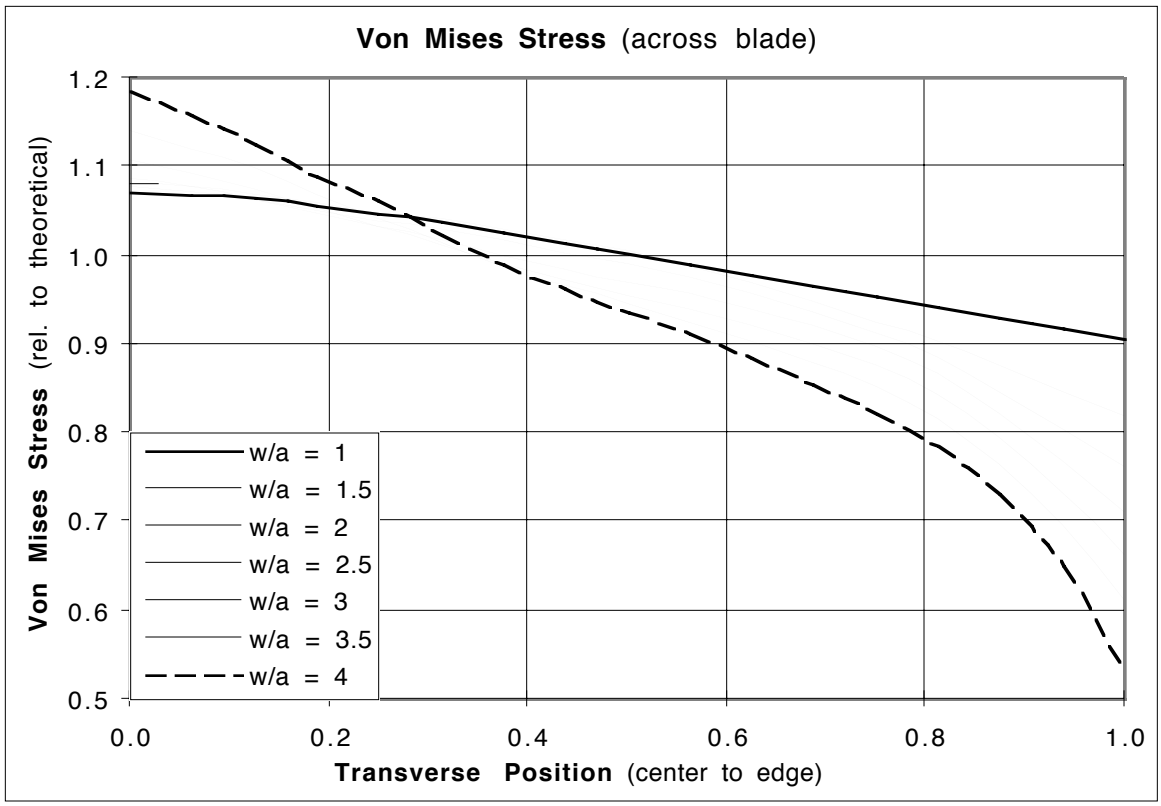

Figure 6-22 Von Mises stress versus position across the half width of the blade (taken at the mid length).

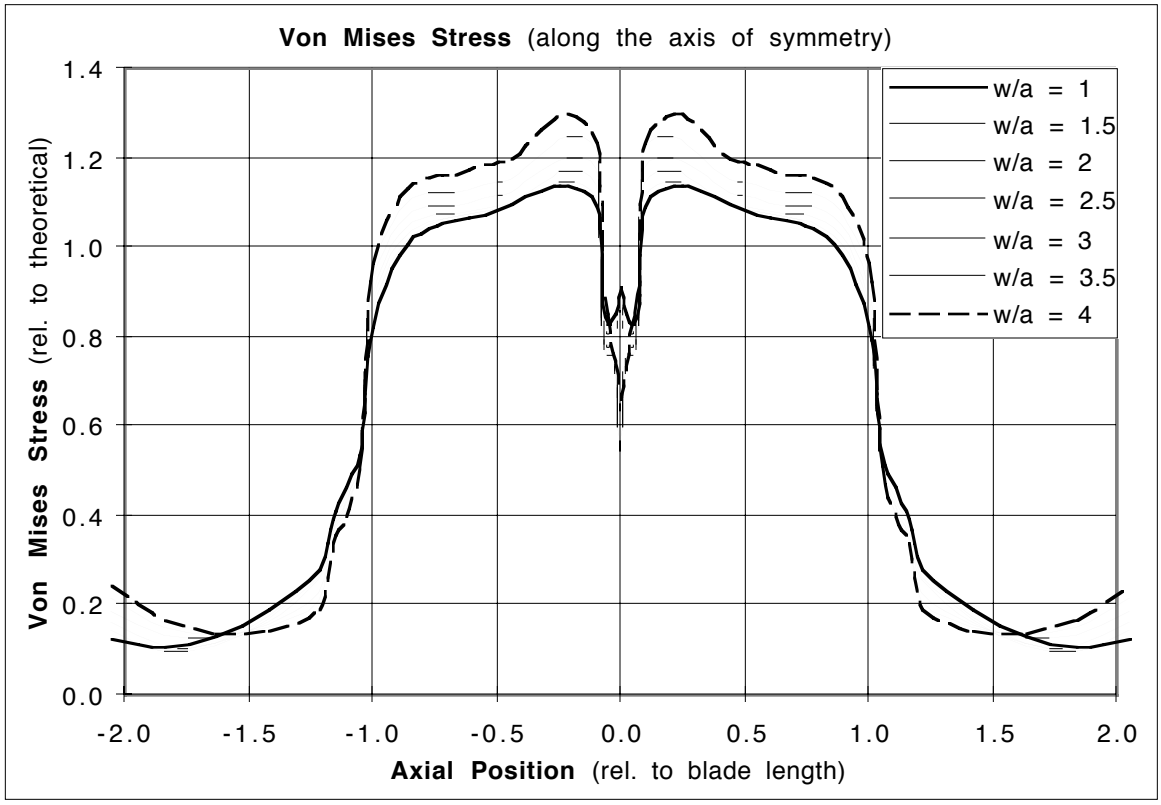

Figure 6-23 Von Mises stress versus position along the axis of symmetry.

6.2.4 Helical Blades for a Ball-Screw Isolation Flexure

The rather specialized application of a ball-screw (or leadscrew) isolation flexure motivated the development of an analytical model for a mildly helical blade flexure. Isolation flexures or bearing systems are commonly used on ultra-precision machines to couple only the desirable degrees of freedom between a ball screw and the carriage it drives [Slocum, 1992]. For different reasons, a recent paper demonstrated a clever way to improve the resolution of a leadscrew by effectively placing a flexural leadscrew in series with the mechanical leadscrew [Fukada, 1996], although no words to this effect are mentioned. While the screw-nut interface requires some level of torque before sliding takes place, the flexural leadscrew responds to arbitrarily small torque to give arbitrarily small resolution. Both of these valuable functions, exact constraint and smaller resolution, can be achieved in one simple device using a set of helical blade flexures. This idea is being used on the NIF precision linear actuator (see Chapter 8.5).

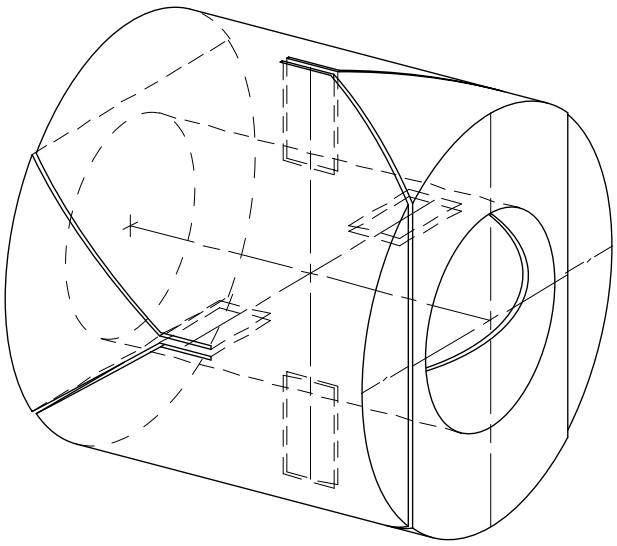

Figure 6-24 The ball-screw flexure for the NIF precision actuator requires two rotational degrees of freedom, a primary constraint against translation along the screw, and secondary constraints for the remaining degrees of freedom. Note, some hidden lines were removed to better show the main features.

Figure 6-24 shows the basic flexure design used for the NIF actuator. It resembles the compact pivot flexure of the last section except that it is hollow to allow the ball screw to pass through. In addition, the two hinge axes intersect to maximally condense the overall length, but this is not required in general. On the NIF actuator, there is another pivot some distance beyond the end of the screw so that the pivot pair provides free translation. Ordinarily the ball-screw flexure would have two pivots to provide free translation. Although it is not apparent from the figure, the blades are manufactured with a slight helix angle. Conceptually, if the blades were concentrated at the pitch diameter of the screw, then the proper helix angle would be perpendicular to the helix of the screw. Since the blades must lie outside the screw, then the actual helix angle must be somewhat smaller. This

condition does two things simultaneously: it aligns the blades to the reaction force; and it aligns out-of-plane motion of the blades to an insensitive direction of the screw. Effectively this creates a flexural screw with the same lead as the mechanical screw. Either one or both can be active since they appear the same to the system.

Before getting into the nature of helical blades, it is instructive to look over the finite-element results in Figure 6-25 for the one-quarter model. The von Mises stress plot in (a) highlights the blades but the point to notice is the gradient across the width. This is an indication of the relative flexibility of the annular junction between the two blades. The axial displacement plot in (b) shows a gradient along the length of each blade and nearly as significant a change in shading through the annular junction. Again this points to the annular junction as being a challenge to make much stiffer than the blades. There is some advantage to using a square cross section rather than an annulus if space permits.

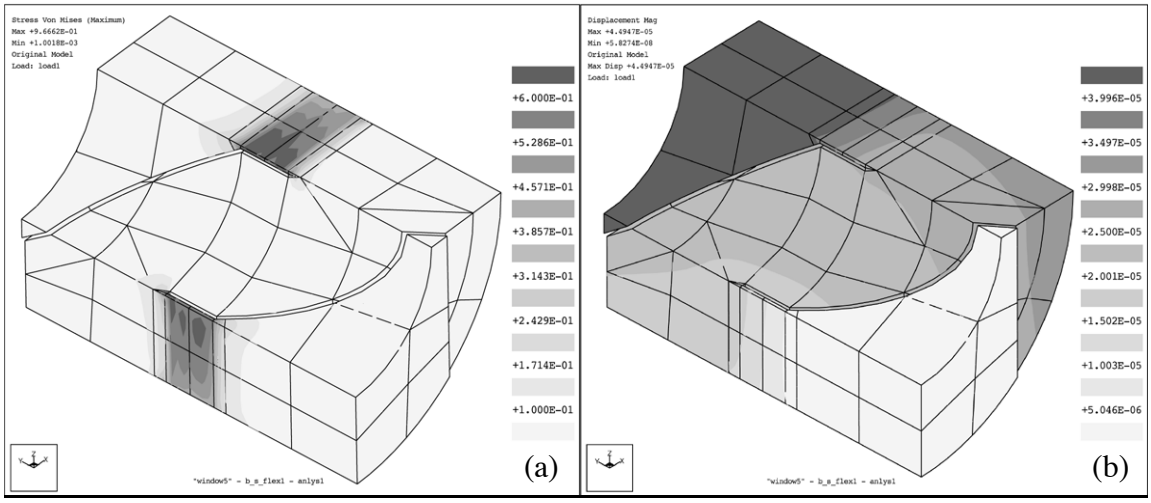

Figure 6-25 Contours of von Mises stress (a) and axial displacement (b) show the basic behavior.

Usually a blade flexure is initially straight so that a small out-of-plane displacement gives only a second-order axial displacement. The helical blade flexure is deliberately inclined with respect to the axis so that a small component of the out-of-plane displacement is along the axis. The angle of inclination varies with radius approximately as $r\,\theta/a$ using the parameters in Figure 6-26. The out-of-plane displacement also varies with radius in a way that compounds with the inclination. Using similar triangles, it is simple to relate the differential motion at any radius to the parameters of the flexure. This relation is then applied to the one particular radius $\bar{r}$ that has no net strain along the blade. The result is the effective lead of the flexure given by Equation 6.10.

$$L \equiv 2\pi \frac{\mathrm{d}x}{\mathrm{d}\theta} = 2\pi \bar{r}^2 \frac{\theta}{a} \tag{6.10}$$

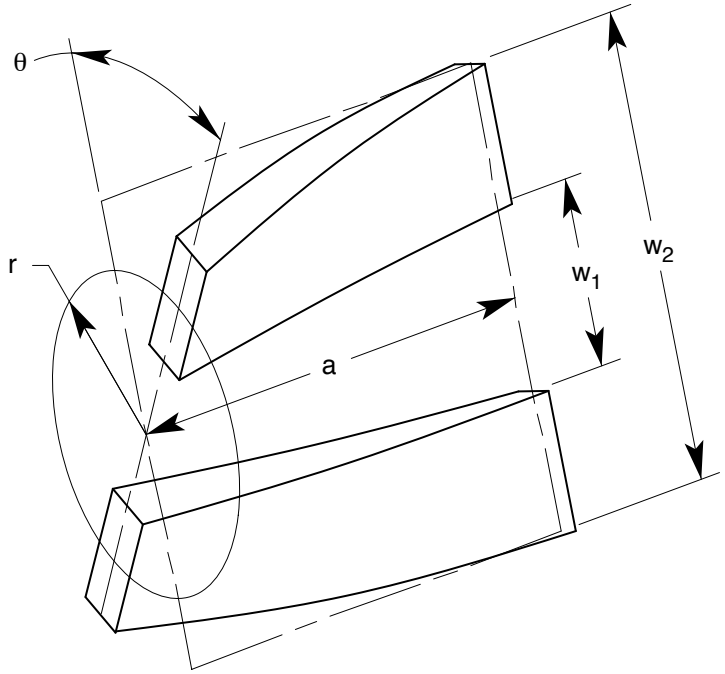

Figure 6-26 The effective lead of a helical blade flexure is governed by the parameters a, w_1, w_2, and θ.

To go further requires an assumption that the ends are constrained to remain parallel. Again using similar triangles, it is simple to determine the axial strain at any radius. Since the flexure is in equilibrium, the axial strain integrated over the cross section must be zero as indicated in Equation 6.11. Upon solving, Equation 6.12 gives the radius for zero strain, which then may be substituted back into Equation 6.10.

$$0 = \int_{r_1}^{r_2} \frac{\partial \varepsilon}{\partial \theta}\, dr = \int_{r_1}^{r_2} \left\{ \frac{\left(r^2 - \bar{r}^2\right)\theta}{a^2 + \left(r\theta\right)^2} \right\} dr \cong \frac{\theta}{a^2 + \left(\bar{r}\theta\right)^2} \int_{r_1}^{r_2} \left(r^2 - \bar{r}^2\right) dr \tag{6.11}$$

$$\bar{r}^2 \cong \frac{1}{3}\left(r_1^2 + r_1 r_2 + r_2^2\right) = \frac{1}{6}\left(w_1^2 + w_1 w_2 + w_2^2\right) \tag{6.12}$$

The axial strain that results from the helical shape also acts to stiffen the flexure in torsion beyond that for a flat blade. The approach used in Equation 6.13 to compute this effect is essentially a strain energy method (Castigliano's first theorem). The additional torsional stiffness due solely to the helix correctly goes to zero as the lead of the screw goes to zero.

$$\begin{aligned} k_{\theta_{helix}} &= 2Eta \int_{r_1}^{r_2} \left(\frac{\partial \varepsilon}{\partial \theta}\right)^2 dr \cong 2Eta \left\{ \frac{\theta}{a^2 + \left(\bar{r}\theta\right)^2} \right\}^2 \int_{r_1}^{r_2} \left(r^2 - \bar{r}^2\right)^2 dr \\ &\cong \frac{Et\left(w_2 - w_1\right)^3}{12a} \left(\frac{4w_1^2 + 7w_1 w_2 + 4w_2^2}{5w_1^2 + 5w_1 w_2 + 5w_2^2} \right) \left\{ \frac{2\pi\bar{r}}{L} + \frac{L}{2\pi\bar{r}} \right\}^{-2} \end{aligned} \tag{6.13}$$

6.2.5 A General Approach for Analyzing Flexure Systems

The most general approach for analyzing a flexure system is finite element analysis. Arbitrarily large, complex systems to very simple systems are readily modeled with commercial FEA software. For example, blade flexures typically modeled with shell elements are connected as necessary to other shell and/or solid elements to represent the whole system. It is hard to imagine a more flexible way to accurately analyze deflections and stresses in some spatially complex arrangement of flexures. Yet in several respects the approach presented here is more flexible than FEA especially early in the design cycle. The model is completely parametric and represents only the elements of interest, usually the flexures. It reports the stiffness and compliance matrices for the constrained system, and it includes column effects that a linear FEA code cannot. The main drawback is that the user must understand the basics of matrix algebra and transformation matrices, which is transparent to the user of an FEA code.

The basic assumption is that the flexure system can be modeled as parallel and series combinations of springs and that an equivalent spring for the system represents useful information, for example, the stiffness matrix. If desired, that information can be propagated back to individual springs, for example, to obtain local forces and moments. The key formalism in this approach is the six-dimensional vector used to succinctly represent three linear degrees of freedom and three angular degrees of freedom. We will deal strictly with force-moment vectors and differential displacement-rotation vectors. These vectors are related through the stiffness matrix or the compliance matrix of the spring. The concept of a three-dimensional stiffness matrix as expressed in Equation 6.14 may be more familiar. The six-dimensional stiffness matrix is assembled as blocks of three-dimensional matrices as Equation 6.15 shows. At times it may be easier to start by building the compliance matrix as in Equation 6.16. Converting from one to the other requires inverting the whole matrix rather than inverting separate blocks.

$$\mathbf{f} = \begin{bmatrix} f_x \\ f_y \\ f_z \end{bmatrix} = \begin{bmatrix} k_{xx} & k_{xy} & k_{xz} \\ k_{xy} & k_{yy} & k_{yz} \\ k_{xz} & k_{yz} & k_{zz} \end{bmatrix} \cdot \begin{bmatrix} \mathrm{d}\delta_x \\ \mathrm{d}\delta_y \\ \mathrm{d}\delta_z \end{bmatrix} = \mathbf{K}_{\mathbf{f}/\delta} \cdot \mathrm{d}\delta \tag{6.14}$$

$$\begin{bmatrix} \mathbf{f} \\ \mathbf{m} \end{bmatrix} = \left[\begin{array}{c|c} \mathbf{K}_{\mathbf{f}/\delta} & \mathbf{K}_{\mathbf{f}/\theta} \\ \hline \mathbf{K}_{\mathbf{m}/\delta} & \mathbf{K}_{\mathbf{m}/\theta} \end{array}\right] \cdot \begin{bmatrix} \mathrm{d}\delta \\ \mathrm{d}\theta \end{bmatrix} \qquad \mathbf{K}_{\mathbf{m}/\delta} = \mathbf{K}_{\mathbf{f}/\theta}{}^{\mathrm{T}} \tag{6.15}$$

$$\begin{bmatrix} \mathrm{d}\delta \\ \mathrm{d}\theta \end{bmatrix} = \left[\begin{array}{c|c} \mathbf{C}_{\delta/\mathbf{f}} & \mathbf{C}_{\delta/\mathbf{m}} \\ \hline \mathbf{C}_{\theta/\mathbf{f}} & \mathbf{C}_{\theta/\mathbf{m}} \end{array}\right] \cdot \begin{bmatrix} \mathbf{f} \\ \mathbf{m} \end{bmatrix} \qquad \mathbf{C}_{\theta/\mathbf{f}} = \mathbf{C}_{\delta/\mathbf{m}}{}^{\mathrm{T}} \tag{6.16}$$

Once the stiffness matrix or the compliance matrix is formed in one coordinate system (CS), it is a simple matter using the [6 x 6] transformation matrix to reflect it to any another (CS). Once expressed in the same CS, stiffness matrices are added to represent

parallel combinations, and compliance matrices are added to represent series combinations. This process is expressed in Equations 6.17 and 6.18 (also A.35 and A.36). Mixed combinations of parallel and series springs require like groups to be combined first then inverted as necessary to complete the combination. See Appendix A for a complete discussion of transformation matrices and parallel and series combinations.

$$\mathbf{K}_0 = \sum_i \mathbf{T}_{0/i} \cdot \mathbf{K}_i \cdot \mathbf{T}_{0/i}{}^{\mathrm{T}} \tag{6.17}$$

$$\mathbf{C}_0 = \sum_i \mathbf{T}_{0/i}{}^{-\mathrm{T}} \cdot \mathbf{C}_i \cdot \mathbf{T}_{0/i}{}^{-1} \tag{6.18}$$

The remainder of this section focuses on the details that make this approach truly useful. The first task is to derive the compliance matrix for the blade flexure. The solution depends on the CS so naturally we will choose the simplest one. Similarly, the stress matrix is derived so that maximum stresses in the blade are easy to calculate. Finally the details of constructing parallel-series spring models are presented.

6.2.5.1 The Compliance Matrix for a Blade Flexure

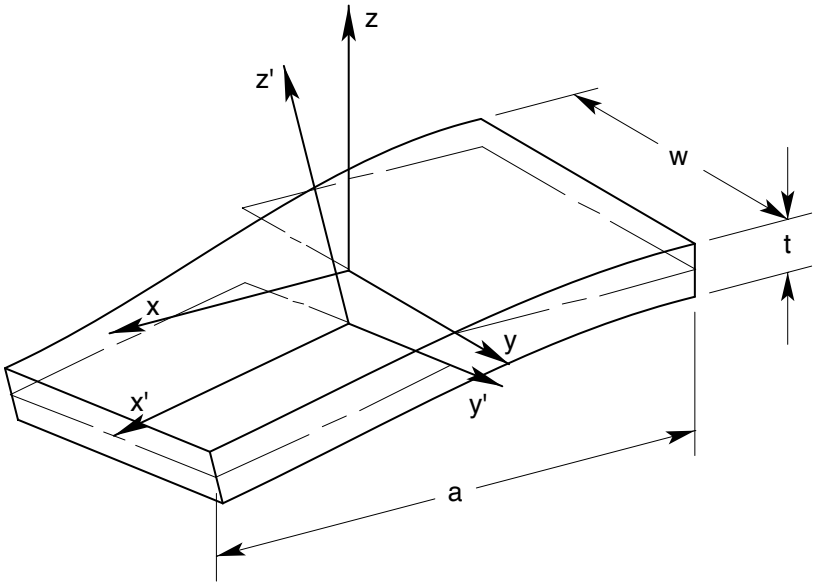

Figure 6-27 Imagining the CS's as rigid links to the ends of the blade, the application of forces and moments at these CS's results in respective displacements and rotations with no coupling between axes.

The flexion of a blade may be represented as movement between two CS's that attach to opposite ends of the blade. It would be more common to place a CS at each end but it is more convenient to place them initially coincident with the principal axes of the blade. Then a blade undergoing flexion appears as slightly displaced CS's in Figure 6-27. In similar fashion, the forces and moments may be represented about these CS's rather than at the ends where they are physically applied. This choice of CS's diagonalizes the compliance

matrix. Four of the six diagonal elements appear already in Chapter 2.6 as stiffnesses but without derivation or explanation. Here we go through each element with due care and add more generality with column effects and side-by-side blades. As in Figure 6-26, w_2 is the outside dimension of blades and w_1 is the inside dimension. In addition, it is necessary to represent the width of the individual blades or of a single blade as w.

We begin with the in-plane constraint directions. Axial compliance is the first diagonal element in the compliance matrix (6.19) and is so familiar that it needs no explanation. It is linear in all the key parameters and therefore is convenient for normalizing the other compliances. The second diagonal element (6.20) corresponds to a y-direction force, which produces combined bending and shear in the blade. It comes from the familiar fixed-guided beam equation and has an added term for the shear deformation. The section properties have been simplified for the side-by-side blade geometry. The last constraint direction is also the last element in the compliance matrix (6.21). Here the blade is in pure bending due to a moment about the z axis.

$$\mathbf{C}_{1,1} = c_x = \frac{a}{E\,t\left(w_2 - w_1\right)} \tag{6.19}$$

$$\mathbf{C}_{2,2} = c_y = c_x \left\{ \frac{a^2}{{w_1}^2 + w_1 w_2 + {w_2}^2} + 2.4\left(1 + \nu\right) \right\} \tag{6.20}$$

$$\mathbf{C}_{6,6} = c_{\theta_z} = \frac{12\,c_x}{{w_1}^2 + w_1 w_2 + {w_2}^2} \tag{6.21}$$

The remaining diagonal elements are out-of-plane directions usually considered as degrees of freedom. The elements corresponding to z and θ_y directions are similar to y and θ_z directions from before and differ mainly in a factor t^2 in the denominator rather than w^2. However, there are two subtle distinctions. As noted earlier in Section 6.2.2, the equations for bending compliance should include a factor $(1 - \nu^2)$ to account for the Poisson effect. The other factor is the effect of an axial force, either compressive or tensile. The solutions for fixed-guided and cantilever boundary conditions are available from numerous sources, for example, [Vukobratovich and Richard, 1988], [Young, 1989] and [Smith, 1998]. Unfortunately the equations are not particularly convenient or intuitive, involving trigonometric functions for compression and hyperbolic functions for tension. Upon substituting power series approximations, the two types of functions become the same when expressed with a positive or negative axial force. The number of terms required in the power series depends upon how closely the flexure operates to the critical buckling load. We will keep enough terms to have good accuracy through one-half the critical load.

The third diagonal element for the z-direction force (6.22) follows from the series approximation of the axially loaded, fixed-guided beam. The effect of the axial force is contained within the square brackets. As expected, the compliance decreases for a positive

tensile force and increases for a negative compressive force. The approximation differs from the exact solution by only 6.6% at one-half the critical load. Usually we would not venture this close to buckling unless the intent is a zero-stiffness condition. Then it is necessary to use the exact solution from the references.

$$\mathbf{C}_{3,3} = c_z \cong c_x \left\{ \left(1 - \nu^2\right)\left(\frac{a}{t}\right)^2 \left[1 - \frac{6}{5}\gamma + \frac{17}{35}\gamma^2 - \frac{62}{315}\gamma^3\right] + 2.4(1+\nu) \right\} \qquad (6.22)$$

$$\gamma \equiv \frac{f_x c_x a}{t^2} \qquad \gamma_{cr} = \frac{\pi^2}{12}$$

The fifth diagonal element corresponds to a moment load applied about the *y*-axis. When an axial force also exists, we must be careful to apply it through the CS rather than at the end of a cantilever beam as in the published solution. Figure 6-28 shows the subtle difference in the way the axial force is applied to the end in (a) and through the CS in (b). The differential equation for the model in (b) has one additional term, $f\ \theta\ (a - x)$. The solution proceeds in a similar way and simplifies for compression to a single sine function rather than a tangent function or the equivalent hyperbolic function for tension. Applying the series approximation results in the fifth diagonal element (6.23). In this case the compliance increases under tension and decreases under compression.

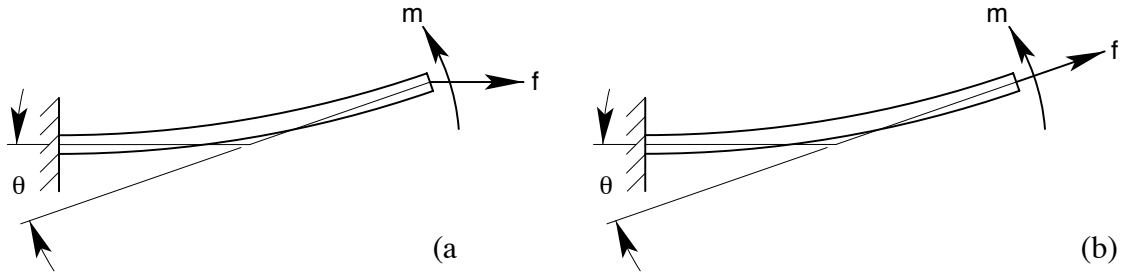

Figure 6-28 The tensile force stiffens the beam in (a) while making it more compliant in (b).

$$\mathbf{C}_{5,5} = c_{\theta_y} = \frac{12\,c_x}{t^2}\left(1 - \nu^2\right)\left[1 + 2\gamma + \frac{6}{5}\gamma^2 + \frac{12}{35}\gamma^3\right] \qquad (6.23)$$

The fourth diagonal element (6.24) corresponds to twisting of the blade. This relation comes from the parallel combination of two effects. The first term within the braces is simple twist with no end effects. This solution is given in several references, for example, [Timoshenko and Goodier, 1951] and [Young, 1989]. The second term brings in the end effects by considering the blade as a series of thin fixed-guided beams distributed across the width. The deflection varies as the radius from the twist axis, and an integration provides the cumulative effect. Since c_z appear in this relationship, it accounts for the Poisson and axial-force effects. This relation agrees well with a parameterized finite-element study.

$$\mathbf{C}_{4,4} = c_{\theta_x} = 12\left\{\frac{1}{2(1+\nu)}\left(4 + 2.52\frac{t}{w}\right)\frac{t^2}{e_x} + \frac{w_1^2 + w_1 w_2 + w_2^2}{c_z}\right\}^{-1} \quad (6.24)$$

6.2.5.2 The Stress Matrix for a Blade Flexure

The distribution of stress through a blade varies greatly depending on the direction of the applied force or moment. For purposes of sizing the blade, however, it is sufficient to consider only the maximum absolute value of stress resulting from applied forces and moments. This information may be represented in a diagonal matrix similar to the compliance matrix. The judicious choice of the CS causes symmetric distributions of stress due to individual components of the force-moment vector. Each distribution will have the maximum absolute value of stress always extending to the eight corners of the blade. There is one worse-case corner where all the stresses are in general alignment (perfectly aligned if not for shear stresses). Then a somewhat conservative estimate of the combined maximum absolute principle stress is the simple sum of the individual maximum's as calculated from the stress matrix multiplied by the applied force-moment vector.

In keeping with the order presented for the compliance matrix, the three terms that correspond to constraint directions are considered first for the stress matrix. The first diagonal element for axial loading (6.25) is simply the inverse of the cross sectional area. It is convenient to use for scaling the other terms. For the second diagonal element (6.26), the *y*-direction force produces combined bending and shear in the blade. A somewhat conservative approach treats the maximum absolute value of principle stress as if aligned with the *x*-axis. This simplifies the final step of combining all the stress components but yields a slightly higher combined stress than a more rigorous analysis. The last constraint direction and also the last element in the stress matrix (6.27) is much simpler because the blade is in pure bending from a *z* moment.

$$\mathbf{S}_{1,1} = s_x = \frac{1}{t(w_2 - w_1)} \quad (6.25)$$

$$\mathbf{S}_{2,2} = s_y = s_x\left\{\frac{3a w_2}{2\left(w_1^2 + w_1 w_2 + w_2^2\right)} + \sqrt{\left(\frac{3a w_2}{2\left(w_1^2 + w_1 w_2 + w_2^2\right)}\right)^2 + 1}\right\} \quad (6.26)$$

$$\mathbf{S}_{6,6} = s_{\theta_z} = s_x\frac{6\,w_2}{w_1^2 + w_1 w_2 + w_2^2} \quad (6.27)$$

The stresses due to the remaining three elements usually result due to required motions of the flexure but they will be written for applied loads. The third diagonal element (6.28) corresponds to a *z*-direction force. Although the blade experiences combined bending and shear loading, the shear stress is usually not significant given normal blade

proportions. It is excluded in preference of keeping a simple expression for the column effect from an axial force. As expected the bending stress increases with a negative compressive force and decreases with a positive tensile force. The fifth diagonal element corresponds to a *y*-moment (6.29) and exhibits slightly more complicated behavior. The axial force causes the bending moment to be nonsymmetric along the length of the blade.[I] The bending moment is maximum at the fixed end for tension and minimum for compression. The use of the singularity function in the equation turns off the effect of a compressive force when γ is negative, leaving just the applied moment as the maximum.

$$\mathbf{S}_{3,3} = s_z = s_x \frac{3a}{t}\left[1 - \gamma + \frac{6}{5}\gamma^2 - \frac{51}{35}\gamma^3\right] \tag{6.28}$$

$$\mathbf{S}_{5,5} = s_{\theta_y} = s_x \frac{6}{t}\left[1 + 6\langle\gamma\rangle^1 + 6\langle\gamma\rangle^2 + \frac{12}{5}\langle\gamma\rangle^3\right] \tag{6.29}$$

As described in the previous section, there are two effects to consider when a blade twists on axis. The first is simple twist with no end effects. The shear stress produced is maximum far away from the corners and therefore may be safely ignored. The other effect is bending of the blade as a fixed-guided beam with the maximum stress occuring at the corners. The fourth diagonal element (6.30) represents this effect by using s_z as the reference rather than s_x. As a result it also represents column effects.

$$\mathbf{S}_{4,4} = s_{\theta_x} = s_z \frac{6\,w_2}{w_1^2 + w_1 w_2 + w_2^2} \tag{6.30}$$

The stress matrix multiplied by the force-moment vector gives a vector of stress components that may be positive or negative depending on the loading. It is useful to look at each component to understand which loads are most significant. The worse-case stress is conservatively estimated by summing the absolute values of the stress components.

6.2.5.3 Parallel-Series Spring Models

The use of parallel and series combinations of springs is fairly common in engineering analysis. Working in 6-D is certainly less common but the basic concept of parallel-series combinations is no different. Most of the gritty details are in the matrix algebra carried out by the computer. The most challenging aspect usually is in setting up the transformation matrices. Perhaps the best way to understand the modeling aspect is to work through an example step by step. The X-Y-θ_Z flexure stage, shown in Figure 6-11 on page 184, is a good example to represent several levels of parallel and series combinations of springs.

[I] The asymmetry of the bending moment is a consequence of the way the blade is loaded along the *x* axis of one CS. A symmetric bending moment would result if the axial force bisected the *x* axes of both CS's. This symmetric case is more appropriate for the cross blade flexure but not for more general arrangements.

Figure 6-29 shows the spring model of the same flexure stage with three actuators. The steps required to set up and analyze the model are enumerated below.

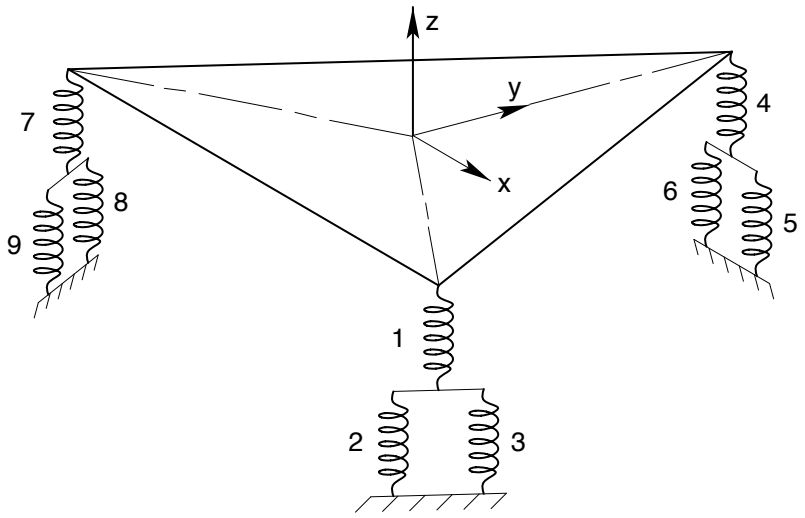

Figure 6-29 The X-Y-θ_Z flexure stage appearing in Figure 6-11 is modeled with nine springs in parallel and series combinations as shown.

j) Identify the main member (the thing being moved or supported) and attach the base coordinate system CS_0 at a convenient location. It is simple to reflect the results to a different CS if desired.

k) Identify all the separate paths from the main member to ground. There are six in the example, three flexure supports and three actuators.

l) Identify and number each spring in each path. There are nine in the example, six blades and three actuators.

m) Assign a unique CS to each spring. Number these CS_1 to CS_n. Then create [6 x 6] transformation matrices to represent the spatial relationships between the local CS's and the base CS_0.

n) Create as many compliance matrices as required to represent all the springs with respect to their own local CS's. There are only two for the example, one matrix for six identical blades and one matrix for three identical actuators.

o) Reflect the compliance matrix for each spring to the base CS_0 using the transformation matrices, thus creating *n* unique compliance matrices. Number these $\mathbf{C}_1$ to $\mathbf{C}_n$.

p) Identify the springs that form either series or parallel combinations. When reflected to the same CS, series springs experience the same load while parallel springs experience the same deflection. The example has three sets of parallel springs, 2-3, 5-6 and 8-9.

q) Add the stiffness matrices of springs in parallel and add the compliance matrices of springs in series. Indicate these new equivalent springs by the spring numbers they represent. The equivalent springs for the example are $\mathbf{K}_{2\text{-}3}$, $\mathbf{K}_{5\text{-}6}$, and $\mathbf{K}_{8\text{-}9}$.

r) Repeat steps 7 and 8 using the equivalent springs in place of the ones they represent. Stop when there is only one equivalent spring remaining. The example requires a total of three combination steps before reaching the equivalent spring for the system. The second step is a series combination resulting in $\mathbf{C}_{1\text{-}2\text{-}3}$, $\mathbf{C}_{4\text{-}5\text{-}6}$, and $\mathbf{C}_{7\text{-}8\text{-}9}$. The last step is a parallel combination resulting in $\mathbf{K}_0$, the equivalent spring for the system.

There are a number of uses for the system stiffness and compliance matrices. Presumably there is some requirement that drives the design to have a certain level of stiffness in the constraint directions and certain freedoms in other directions. Specific load cases may be applied to ascertain deflections or certain motions may be specified to determine resulting reaction forces. The sizes and locations of blades are easily modified to evaluate design changes. Details about individual blades such as stresses or reaction forces require the applied load or specified motion to be propagated back through the combination process, being careful to apply loads to springs in series or motions to springs in parallel. A clearly labeled sketch of the model for each step in the combination process will help avoid confusion and mistakes.

The fine details of these analysis steps appear in the flexure system analysis program in Section 6.3. The program documents the example of the X-Y-θ_Z flexure stage discussed here. In particular it shows how to set up the [6 x 6] transformation matrices and reflect compliance matrices to the base CS_0. It also shows how easily a fairly complex system of blades is modeled with parallel and series combinations of springs.

A slightly more advanced topic is the modeling of column effects in a system of flexures. It was not an important effect in the X-Y-θ_Z flexure stage so it was not introduced then. The compliance matrix and the stress matrix for individual blades account for local column effects, but it is necessary to include the system effects at the system level. Fortunately this is straightforward to do with additional springs that represent the column behavior. This behavior may occur when a series combination carries a significant axial force, for example, when two blades lie in the same plane so as to act like one much longer blade. The effect of the axial force is modeled with a new spring placed in parallel with the series combination. The stiffness of the new spring depends only on the axial force and the distance between the two CS's of the series combination, as in Equation 6.31. It may be positive or negative for a tensile or compressive force, respectively. When reflecting this stiffness to the base CS_0, the transformation matrix should be the same as the most mobile blade in the series combination. Then it may be combined as any of the other springs.

$$\mathbf{K}_{3,3} = \frac{f_x}{L} \tag{6.31}$$